

NDT-59770  
NASA CR 104096

# RADIATION PYROMETER FOR LUNAR OBSERVATION



CASE FILE  
COPY

by

HECTOR C. INGRAO AND DONALD H. MENZEL

HARVARD COLLEGE OBSERVATORY  
CAMBRIDGE, MASS., U.S.A.

NASA RESEARCH GRANT NO. NGR 22-007-001

Formerly Grant No. NSG 64-60

APR 1 1963

PREPARED FOR THE

NATIONAL AERONAUTICS AND SPACE ADMINISTRATION

RADIATION PYROMETER FOR LUNAR OBSERVATION

by

Hector C. Ingrao and Donald H. Menzel

Harvard College Observatory  
Cambridge, Massachusetts (USA)

NASA RESEARCH GRANT NO. NGR 22-007-001

Formerly Grant No. NSG 64-60

**APR 1 1969**

Prepared For The  
NATIONAL AERONAUTICS AND SPACE ADMINISTRATION

# RADIATION PYROMETER FOR LUNAR OBSERVATION

by

Hector C. Ingrao and Donald H. Menzel

## ABSTRACT

This report analyzes a radiation pyrometer for lunar observations, developed at the Harvard College Observatory.

One of the criteria for designing this pyrometer was the utilization of thermal detectors for developing techniques suitable for space instrumentation, and to make observations possible outside the United States. Moreover, the astrometric aspects of the radiometric measurements in this radiation pyrometer were seriously considered.

The pyrometer has three channels: infrared, photographic (astrometric purposes), and visual. All three channels use the same telescope optics and are commutated by a two-sided mirror chopper. The pyrometer head has plug-in units, making possible the use of different thermal detectors, photomultiplier tubes, and a focusing test unit.

The location of the resolution element on the lunar surface could be achieved within three seconds of arc, or one-third of the resolution element. The noise level of the pyrometer, under certain conditions, is  $6 \times 10^{-11}$  watts peak-to-peak for one second post-detection integration time.

Detailed descriptions of the electro-mechanical parts of the radiation pyrometer and its electronic circuitry are given, since a great deal of effort was put into the design of these parts.

## CONTENTS

<u>I.</u>	<u>INTRODUCTION</u>	1
<u>II.</u>	<u>ASTRONOMICAL OBJECTIVE</u>	3
A.	Observational Problem	3
B.	Spatial Resolution	5
C.	Identification of the Resolution Element on the Lunar Surface	7
D.	Temperature Resolution on the Lunar Surface	13
<u>III.</u>	<u>RADIATION PYROMETER SYSTEM</u>	18
A.	General Description	18
B.	Pyrometer Head	18
1.	Variable Speed Chopper Subassembly	23
a.	Glass Chopper	23
b.	Chopper Shaft Subassembly	28
c.	Clutch	28
d.	Variable Ratio Speed Changer	29
e.	Flexible Shaft Coupling	29
f.	Electric Motor	29
g.	Test of the Variable Speed Chopper.	30
2.	Reference Blackbody	30
3.	Calibration Blackbody	34
4.	Thermistors	37
5.	Optical Filters	37
a.	Infrared	37
b.	Visible	40
6.	Focusing Compensator	40
7.	Reticle	45

## CONTENTS (Continued)

8.	Photographic Camera . . . . .	45
9.	Phase Sensor . . . . .	46
10.	Plug-In Units . . . . .	47
	a. Visible . . . . .	47
	b. Focusing and Foucault Test . . . . .	49
	c. Infrared . . . . .	53
	c.1. Thermistor Bolometer . . . . .	54
	c.2. Preamplifier . . . . .	59
C.	Electronic Console . . . . .	61
	1. Voltage Monitor . . . . .	61
	2. Phase Controlled Rectifier . . . . .	61
	3. DC Vacuum Tube Voltmeter, Bucking Signal and Time Constant . . . . .	64
	4. Paper Chart Amplifier-Recorder . . . . .	68
	5. Thermistor Thermometer . . . . .	69
	6. Picture Frame Counter and Calibration Blackbody Temperature Adjustment . . . . .	74
	7. Power Distribution . . . . .	74
D.	Monitor Console . . . . .	75
	1. Magnetic Tape Recorder . . . . .	75
	2. Digital Clock . . . . .	75
	3. Radio Receiver for Time Signals . . . . .	76
	4. Intercommunication System . . . . .	77
	5. Event Signal . . . . .	77
IV.	<u>TEST AND CALIBRATION</u> . . . . .	78
	A. Noise Level, Linearity and Drift of the Pyrometer . . . . .	78
	B. Test of the Pyrometer-Telescope System . . . . .	80

CONTENTS (Continued)

C.	Blackbody Thermistor Thermometers	
	Calibration . . . . .	84

<u>REFERENCES.</u> . . . . .	88
------------------------------	----

## CONTENTS (Continued)

### FIGURES

- 2-1. Size of the field of view and the size in miles (or kilometers) of the resolution element on the moon as a function of the telescope focal length; a.) for detector with 1 mm x 1 mm effective size, b.) for detector .35 mm x .35 mm in size . . . . . 6
- 2-2. Measurement of the radiation pyrometer profile: a.) frames 1 to 4 show Alpha Scorpii crossing the field of view of the photographic channel of the radiation pyrometer along one line of the reticle; b.) output of the radiometric channel when Alpha Scorpii crossed the field of view . . . . . 6
- 2-3. Basic principle of the mechanism for identifying the resolution element on the lunar disk in the radiation pyrometer developed at the Harvard College Observatory. . . . 9
- 2-4. Picture obtained with the photographic channel of the radiation pyrometer, using E, G&G-XR film, Wratten #15 filter and an exposure time of 1/15 second. The center of the reticle is on the south tip of Mare Crisium. . . . . 9
- 2-5. Film analyst making initial identification of a lunar region in one picture frame using a high contrast photograph of the moon. In the background the projection screen mounted on a gimbal; in the foreground the film projector mounted on a structure with three degrees of freedom. The rotation of the projector head gives the fourth degree of freedom . . . . . 11
- 2-6. Schematic of configuration pyrometer-telescope-moon to compute the infrared signal on the detector of the radiation pyrometer (the secondary mirror of the telescope has been omitted to simplify the drawing) . . . . . 14
- 3-1. Block diagram of the radiation pyrometer system . . . . . 19
- 3-2. Photograph of the electronic console, monitor console and paper chart recorder of the radiation pyrometer developed at the Harvard College Observatory for lunar observations . . . . . 20
- 3-3. Schematic of the pyrometer head. . . . . 22
- 3-4. View of the pyrometer head with the side plate removed . . . 24

## CONTENTS (Continued)

### FIGURE

3-5.	Isometric view of the complete variable speed chopper subassembly. . . . .	25
3-6.	Chopper holder and adjustment mechanism. . . . .	27
3-7.	Schematic of the reference blackbody . . . . .	31
3-8.	Views of the reference blackbody before insulation; a.) from the guide plate side, b.) from the aperture stop side . . . . .	33
3-9.	Schematic of the calibration blackbody . . . . .	35
3-10.	Cross-section of the thermistor assembly units. . . . .	35
3-11.	Spectral transmittances $\tau(\lambda)$ of 1) wide-bandpass filter detector window combination, and 2) narrow-bandpass filter detector window combination. Predicted spectral atmospheric transmittance $\tau_A(\lambda)$ based upon our model for 10 mm of precipitable water and $m=1$ . Regions of the spectrum with the important absorbing constituents are marked. (The region between 12.54 and 13.0 $\mu$ has been interpolated.) . . . . .	39
3-12.	Spectral radiant transmittance of the two multilayer interference filters for the visible channel of the radiation pyrometer . . . . .	39
3-13.	Focusing compensator mechanism . . . . .	41
3-14.	Effect in the focusing produced by the insertion of filters or compensating plates in the optical path; a.) immersion lens, b.) filter or compensating plate . . .	43
3-15.	Schematic of the photomultiplier and HV supply plug-in unit . . . . .	48
3-16.	Ray tracing for the Foucault test plug-in unit . . . . .	50
3-17.	Schematic of the focusing Foucault test plug-in unit . . .	52

## CONTENTS (Continued)

### FIGURE

3-18.	Schematic of the circuit used for the thermistor bolometer bridge. . . . .	58
3-19.	Circuitry of the Barnes Engineering transistor preamplifier Model DP-5A. . . . .	60
3-20.	Circuit of the phase controlled rectifier . . . . .	62
3-21.	To check the phase controlled rectifier performance, the test unit generates a dummy signal and reference voltages at fixed frequencies and continuous variable phase difference. . . . .	65
3-22.	Oscillograms of the input and output signals of the PCR for different conditions of operation: a) input signals from the photodiode at 2.5, 6 and 32 Hz (scale 1 V cm <sup>-1</sup> ); b) output for 180°, 270° and 0° phase angle difference at 2.5 Hz (scale .05 V cm <sup>-1</sup> ); c) output for 80°, 270° and 0° phase angle difference at 32 Hz (scale .05 V cm <sup>-1</sup> ) and d) response for input step scale .05 V cm <sup>-1</sup> ) . . . . .	66
3-23.	Simplified circuitry of a thermistor constant sensitivity bridge . . . . .	70
3-24.	Circuit diagram of the thermistor thermometer to measure the calibration and reference blackbody temperatures . . . . .	72
4-1.	Noise level and drift measurement of the radiation pyrometer. . . . .	79
4-2a.	First part of a complete lunar scan, time identifying pictures, signal marks, and marks indicating when a picture has been secured. Data obtained during the Lunar Eclipse, December 18-19, 1964, with the 155 cm (61 in.) telescope at Agassiz Station. The total amount of precipitable water in the Earth's atmosphere was 1.4 mm. This part of the scan went through an area in penumbra . . . . .	81

## CONTENTS (Continued)

### FIGURE

- 4-2b. Continuation of data and scan shown in Fig. 4-2a.  
This part of the scan passed almost through the  
Center of Copernicus during the umbral phase.  
The  $\Delta T$ 's are not corrected by instrumental profile. . . . . 82
- 4-3. Scan and time marks a few hours before the Lunar  
Eclipse of June 24-25, 1964, observed from Pretoria  
(Rep. of South Africa) with the 188 cm (74 in.)  
telescope. The scan shows several temperature  
anomalies. To show the validity of the measure-  
ments, the direction of scanning was reversed.  
The second scan shows an almost perfect mirror  
image of the first scan. The  $\Delta T$ 's are not correct-  
ed by instrumental profile . . . . . 83
- 4-4. Calibration setup for the thermistor thermometers . . . . . 85

## I. INTRODUCTION

The present report covers the design criteria and principles, detail of construction, and performance of a radiation pyrometer for lunar work presently used by Harvard College Observatory at different observing sites.

In many instances, the theoretical performance of an infra-red detecting system is not achieved because poor design or construction, (i.e., vibration from the chopper), tend to impair the results expected from the pure thermodynamic analysis of the detector. This report describes in some details, therefore, the physical realization of parts of the pyrometer which we consider critical in this respect.

We were stimulated by NASA's need for reliable equipment to obtain thermal lunar data with high temperature and spatial resolution, including the ability to identify accurately the area under measurement at any time.

The initial problem was to determine the detector best-suited for the job. Our Scientific Report No.1<sup>1</sup> attempted to determine this. The final decision about the detector was made not only on the basis of the minimum NEP, but also, its ruggedness, sensitivity to vibration, changes in signal-to-noise ratio caused by changes in the temperature of the environment, etc., were considered. We wished to choose equipment that could be operated outside the United States, and to develop techniques that could be easily extrapolated to space instrumentation. This practically ruled-out quantum detectors, since operating them in the wavelength range of  $8\mu$ - $14\mu$  (depending upon the type of detector) requires the use of liquid helium or other liquefied gases which are difficult to obtain outside the USA (Unclassified - State-of-the-Art, 1961).

We concluded that the immersed thermistor bolometer was, at this time, the best-suited for part of this application. To overcome some of the drawbacks that existed, we began parallel development of a new type of detector, the ferro-electric bolometer<sup>2,3,4</sup>.

We wanted to have modular equipment, so that by changing modules we could use different detectors and associated electronics to do photoelectric photometry in the visible range.

To achieve our objective we designed our own equipment, considering carefully the design and craftsmanship in order to make sure at each stage that we were within the limits of the State-of-the-Art.

We should like to point out as a novel aspect of this equipment the mechanism which allows for accurate location of the area under measurement. Moreover, we would like to emphasize the variable speed drive for the chopper which allows for different scanning rates or time constants and the focusing mechanism of the pyrometer head.

## II. ASTRONOMICAL OBJECTIVE

### A. Observational Problem

The type of lunar temperature measurements made and the methods used will be determined solely by the information we want to obtain from the data; the choice of high or low spatial resolution, high or low temperature resolution, and relative or absolute measurements can be made only on the basis of the answers we were seeking for our program.

For example, to correlate radio measurements with infrared measurements, instruments with resolution elements of several minutes have been used. With these instruments it is no problem to locate the area under measurement within a fraction of the resolution element. However, if the program calls for high spatial resolution, and one expects to correlate the thermal features with the lunar visual features, the observational and instrumental problem is completely different. For example, if the resolution element is 9" x 9" in size, its accurate location is very difficult and, in fact, requires us to solve an astrometric problem.

At high spatial resolution the stability requirements of the telescope are more demanding. If the moon is being scanned, we must be able to determine the position of the resolution element on the lunar surface as a function of time, and within a fraction of the resolution element size.

Temperature resolution can be a serious problem, depending upon the dynamic range that our equipment has to handle and the time allowed for a complete measurement. A scan during full moon and through the subsolar point must handle a power signal ratio of the order of 270, if we assume two extreme temperatures,  $-123^{\circ}\text{C}$  ( $150^{\circ}\text{K}$ ) and  $+127^{\circ}\text{C}$  ( $400^{\circ}\text{K}$ ). If the noise level of the pyrometer is of the order of  $5 \times 10^{-11}$  watts and if we want the measurements to be limited only by this noise

level, we have to resolve 3 parts in 1000 at +127°C (400°K). Rather complex equipment is needed to handle this amount of information.

The probable error in the absolute temperature measurements will depend mainly on the accuracy of the measurements of the instrumental parameters and of the atmospheric attenuation.

For measurements of relative temperatures, knowledge of the instrumental parameters is not so important, and less accuracy is required in measurements of the atmospheric attenuation.

In our program of lunar temperature measurements, we have designed and built a radiation pyrometer at Harvard College Observatory. This instrument was designed to provide high spatial resolution, high accuracy in locating the resolution element on the lunar surface, and the highest temperature resolution achievable with thermal detectors. The pyrometer has three channels: infrared, visual and photographic. All three channels use the same telescope optics; an optical switching mechanism allows one to observe the moon 50% of the time in the infrared and 50% of the time in the visual range; and, photographically, at an adjustable rate from 10 Hz to 70 Hz. The pyrometer has the following data outputs:

1. A 35 mm film having a field of view 7!5 x 5!0 with a crosshair centered on the frame which coincides with the barycenter\* of the infrared detector;
2. a paper chart on which is recorded the infrared signal, the time, the moment when a picture has been secured, and an event which should be recorded; and,

---

\* We define the barycenter as the point in the detector with the highest responsivity.

3. a magnetic tape recording of the observer's description of the area under measurement, or of any event important to the data analysis. In addition, the operator of the electronic equipment records relevant data on the magnetic tape, plus WWV time signals, and a tone which alerts the operator that an event should be recorded.

#### B. Spatial Resolution

In our radiation pyrometer the size of the resolution element will be limited by the telescope optics, the detector size, the atmospheric seeing, and the seeing conditions at the observing site. If our measurements are in the range of  $8\mu$  to  $14\mu$  and we can assume  $10\mu$  as the effective wavelength, and if we are using a 152 cm (60 in.) telescope, the diameter of the Airy disk is  $3''.3$ ; that of the second dark ring of the diffraction pattern is  $6''.0$ ; and, that of the third is  $8''.7$ . About 94 percent of the total flux falls within the third diffraction ring of an unobstructed circular aperture. On this basis we established as a requirement that the detector should cover at least the third ring of the diffraction pattern; this means that for a telescope with a scale of  $s=25''/\text{mm}$ , the detector should be of the order of 0.35 mm in size. The thermistor bolometer used in our pyrometer, 0.1 mm x 0.1 mm in size and immersed in a germanium lens, gives an effective size of 0.35 mm x 0.35 mm. Since the exit stop of the pyrometer-telescope system is determined by the size of the detector, the spatial resolution will be defined (for a given detector size) by the focal length of the optical system. Figure 2-1 gives the size of the resolution element ( $\Delta L \times \Delta L$ ) in seconds of arc, miles, and in kilometers on the lunar surface at earth-moon mean distance versus focal length of the optical system. To obtain the instrumental profile experimentally, in one set of measurements, we scanned the field of view of our radiation

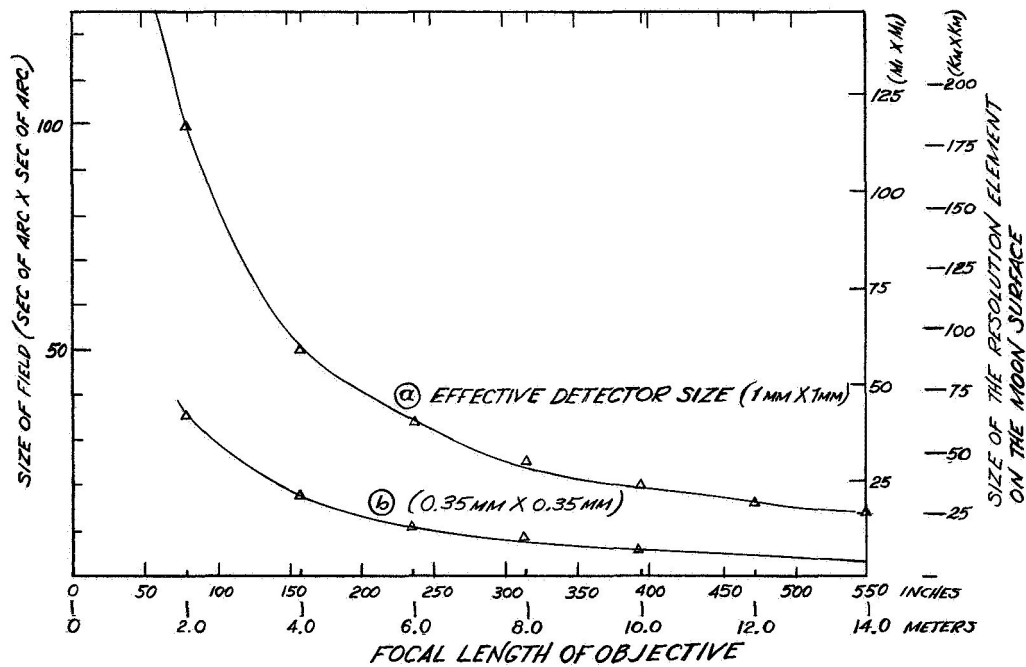


FIG. 2-1. Size of the field of view and the size in miles (or kilometers) of the resolution element on the moon as a function of the telescope focal length; a.) for detector with 1 mm x 1 mm effective size, b.) for detector .35 mm x .35 mm in size.

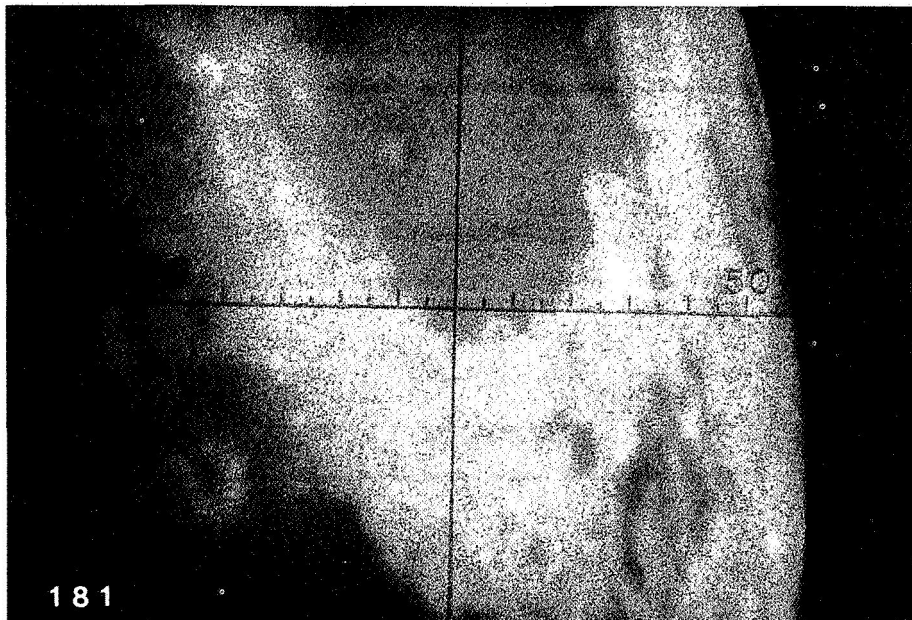


FIG. 2-2. Measurement of the radiation pyrometer profile: a.) frames 1 to 4 show Alpha Scorpii crossing the field of view of the photographic channel of the radiation pyrometer along one line of the reticle; b.) output of the radiometric channel when Alpha Scorpii crossed the field of view.

pyrometer with the image of a star, Alpha Scorpii, and the pyrometer mounted at the Newtonian focus of the 188 cm (74 in.) telescope at the Radcliffe Observatory (Republic of South Africa). Figure 2-2a. shows the photographic record; each small division of the reticle is equivalent to 11". Frames 1 to 4 show Alpha Scorpii crossing the field along the horizontal line of the reticle. The time when the picture was secured is indicated in the upper part of each frame. The film used was E, G&G-XR, the chopping frequency 14 Hz, and the shutter speed, 1.0 second. Figure 2-2b. shows the output of the radiometer when Alpha Scorpii scanned the detector. The marks 1, 2, 3, and 4 indicate the times at which the identifying pictures were secured. The measurements were taken nearly along the diagonal of the square detector.

A series of similar scans was obtained parallel to the horizontal line of the reticle and spaced only a few seconds of arc apart. Using these measurements we determined the size of the resolution element, the responsivity diagram of the pyrometer-telescope combination, and, in addition, any systematic error in the location of the barycenter of the detector with respect to the center of the reticle. On the basis of the record shown in Figure 2-2b. we measured a resolution element 8" x 8" between 50 percent power points.

#### C. Identification of the Resolution Element on the Lunar Surface

The main difficulty in high spatial resolution pyrometry is the problem of identifying the resolution element on the lunar disk. Observations of high spatial and temperature resolution must be obtained, in general, with reflectors of fairly large aperture -- 122 cm (48 in.) and larger. The use of two independent optical systems, one to identify the resolution element and the other for pyrometry, introduces the difficult problem of keeping both optical axes collimated at different attitudes of the telescope; errors can be of the

order of minutes of arc.

However, schemes can be devised to solve this problem and, without discussing the advantage and disadvantages of the several methods used, we will describe the one used in our pyrometer. The basic principle is indicated in Figure 2-3. The equipment is designed to operate with optical systems with f-numbers between 3.5 and 6. The telescope beam is chopped at a rate which can be adjusted from 10 Hz to 70 Hz. The chopper is made of glass and has evaporated aluminum on the front face and evaporated gold on the back.

When the chopper blocks the optical path to the detector in position D, the focal plane d-d' is transferred to the position k'-k. We can call the point R the homologue of the point D that defines the geometrical center of the detector. Coplanar with the image plane k'-k is a reticle with 1/2 millimeter divisions, illuminated at the edge. A flat mirror, E, folds back the beam and the photographic objective, L, images the plane k'-k onto the photographic film. A reflex system with mirror, M, and a pentaprism allows for visual observation of the same field of view.

After the chopper has been made perpendicular to the axis of rotation by means of an autocollimator, the whole optical train is adjusted. For this adjustment we have an auxiliary optical system that is attached to the pyrometer head flange and gives a point image on, D, which, by means of a chopper, can be transferred to R.

For the sake of simplicity we will consider the reticle alignment a two-dimensional problem; it is, in fact, a three-dimensional one.

If we assume that the plane of the mirror chopper has been fixed and that the position D of the detector is determined,

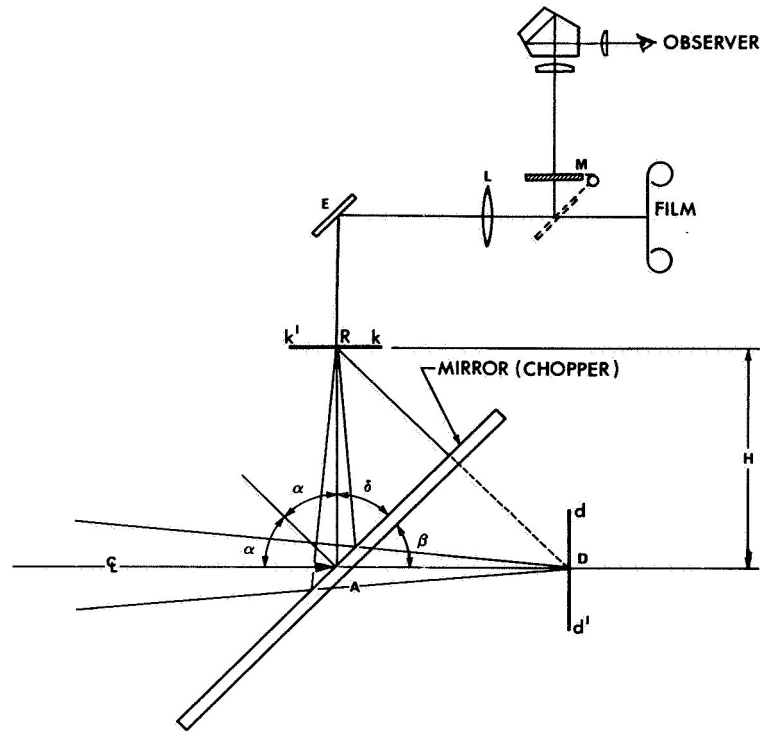


FIG. 2-3. Basic principle of the mechanism for identifying the resolution element on the lunar disk in the radiation pyrometer developed at the Harvard College Observatory.

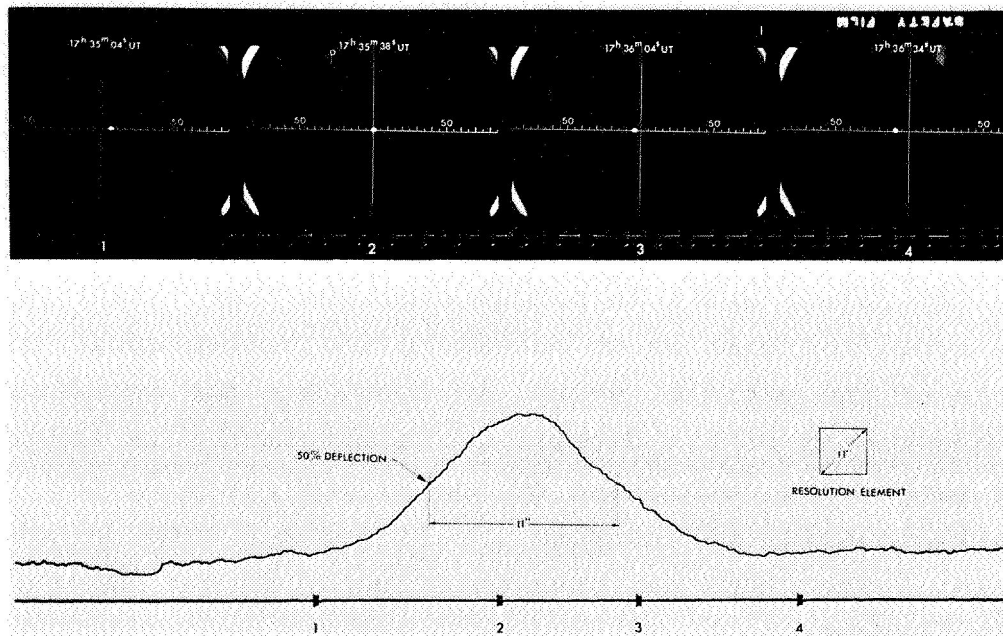


FIG. 2-4. Picture obtained with the photographic channel of the radiation pyrometer, using E, G&G-XR film, Wratten #15 filter and an exposure time of 1/15 second. The center of the reticle is on the south tip of Mare Crisium.

the homologue point R is defined. Since  $\gamma=\beta$  for any  $\alpha$ , the alignment will depend only upon the relative positions of D, the chopper and R.

This method, because of the design of the pyrometer head, could produce a systematic error in the positioning of D. There is always an error in the positioning of the detector flake with respect to the detector holder, which makes the position of D indeterminate. Since we assume that the position of D is known for the alignment in the laboratory, a systematic error is introduced in the positioning of the reticle. Moreover, since the pyrometer head is designed for use with different detectors, we should expect a different systematic error for each detector.

To determine the systematic error at the telescope, we scanned the detector several times with a star image in a direction parallel to the diagonals (square detector) until we got the maximum response. If we correlate photographically the position of the star image on the reticle with maximum signal output from the detector, we can measure the systematic error very accurately.

Figure 2-4 shows an actual picture taken with the photographic channel of the pyrometer. The picture was secured a few minutes before a total eclipse, using E, G&G-XR film plus Wratten #15 filter and 1/15 second exposure time. With pictures of this type, the task is to determine the orthographic coordinates of the reticle, which, in turn, are the coordinates of the barycenter of the detector. We obtained this information by projecting each frame on the proper plate of the Orthographic Atlas of the Moon . \* Figure 2-5 shows a special projecting system that has been constructed in our laboratory for this purpose.

---

\* Orthographic Atlas of the Moon, The University of Arizona Press, 1961.



FIG. 2-5. Film analyst making initial identification of a lunar region in one picture frame using a high contrast photograph of the moon. In the background the projection screen mounted on a gimbal; in the foreground the film projector mounted on a structure with three degrees of freedom. The rotation of the projector head gives the fourth degree of freedom.

The foreground of Figure 2-5 shows the Leitz film projector which is mounted on a structure having 3 degrees of freedom. The projector head can be rotated 360 degrees. As seen in the background of Figure 2-5, the image is projected onto a screen mounted on a gimbal to simulate to first order the librations of the moon. After studying the projected frame, the film analyst must locate the exact area on a photograph of the moon so that the appropriate plate from the Photographic Lunar Atlas\* can be chosen. The projected image is then superimposed on the correct Lunar Atlas plate. In order to ascertain whether the superimposed image is identical to that on the plate, a sheet of white opaque paper is held over the screen and moved around while the outstanding features are lined up with the photographic plate. The point where the reticle crosses is marked on the plate, and is then transferred to the corresponding orthographic plate. The  $\xi$  and  $\eta$  coordinates are determined and recorded in tabular form along with the number of the picture frame. These coordinates will be used later in a computer program to determine the coordinates of the barycenter of the resolution element as a function of time. Because we have less varied illuminations of the moon on Orthographic Atlas plates than on Photographic Atlas plates, we must ordinarily use the Photographic Atlas Plates for the initial plotting of coordinates.

The accuracy in determining the orthographic coordinates of the barycenter of the resolution element depends upon the quality of the raw data. For pictures obtained under good conditions (seeing disk 2" or smaller), having good contrast and a reasonable number of identifiable lunar features, the standard deviation in the determination of the orthographic coordinates is  $\pm 3''$ . For pictures obtained under poor seeing conditions (5" or larger), having poor contrast and few identifiable features, the standard deviation will be between 6" and 8".

---

\* Photographic Lunar Atlas, The University of Chicago Press, 1960.

Usually, we take about four pictures per scan; the best results gave the position of the line of scan within  $1''.5$  and in the average within  $4''.0$ .

In the reduction of the positional data we account for the differential refraction due to atmospheric dispersion between the infrared and the visible rays.\*

The previous discussion regarding the location of the resolution element applies only to the illuminated part of the moon. On the basis of these measurements, we can also determine the position of the line of scan on the shadowed areas. The problem of location on the eclipsed moon is more complicated, especially during dark eclipses. Still, in some cases, it is possible to take the identifying pictures with high-speed film or an image converter, or to take the pictures at the limb of the moon against the star background. In the last case, the position of the line of scan on the moon will be found from the position of the reticle with respect to a given set of background stars.

#### D. Temperature Resolution on the Lunar Surface

For a telescope-pyrometer system operating under ideal conditions the limiting noise should be the statistical fluctuations of the equivalent temperature of the atmosphere or (and) the irreducible noise of the infrared detector.

Based on the geometry shown in Figure 2-6,\*\* the relationship between the radiant power  $I_M$  measured by the pyrometer and the lunar radiance, for an area of orthographic coordinates,  $(\xi, \eta)$ , at a temperature,  $T$ , is given by:

---

\* Analysis of this problem appears in Scientific Report No. 6.

\*\* To simplify the drawing the secondary mirror of the telescope has been omitted.

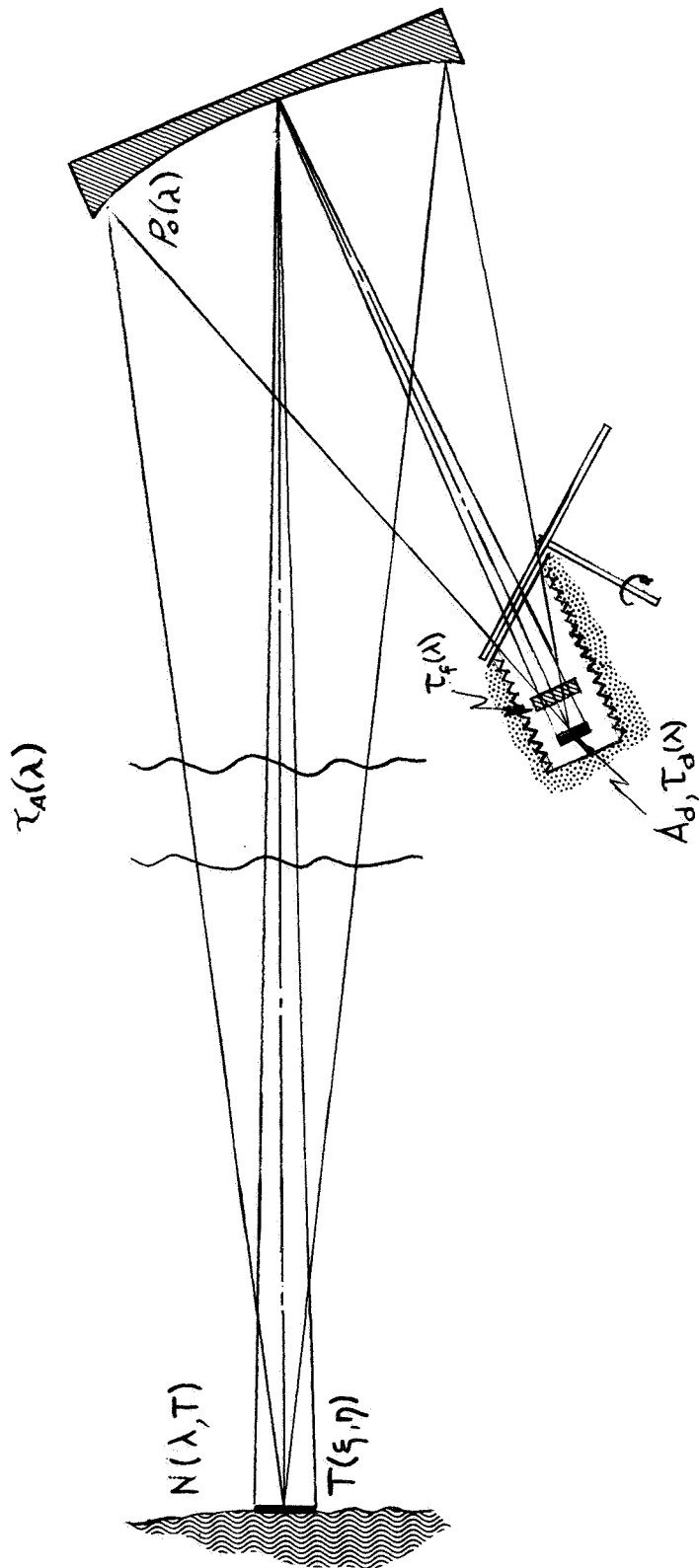


FIG. 2-6. Schematic of configuration pyrometer-telescope-moon to compute the infrared signal on the detector of the radiation pyrometer (the secondary mirror of the telescope has been omitted to simplify the drawing).

$$I_M = \frac{A_d \rho_0^2}{4F_{eff}^2} \bar{\tau}_A [T(\xi, \eta), m, \omega] S[T(\xi, \eta)] \quad , \quad (2-1)$$

where

$A_d$  = area of the detector,  $\text{cm}^2$ ,

$\rho_0$  = radiant reflectance of the mirror (aluminized) of the telescope; there are two mirrors, thus the effective reflectance is  $\rho_0^2$ ,

$F_{eff}$  = effective f-number of the optical system during measurements

$\bar{\tau}_A [T(\xi, \eta), m, \omega]$  = mean atmospheric radiant transmittance,

$T(\xi, \eta)$  = brightness temperature,  $^{\circ}\text{K}$ ,

$m$  = air mass along the line of sight

$\omega$  = amount of precipitable water along the path, mm,

$S[T(\xi, \eta)]$  = radiance corrected for instrumental transmittance and radiant emissivity,  $\epsilon_M$ , of the lunar surface,  $\text{W cm}^{-2} \text{sr}^{-1}$ .

Taking the radiance  $S[T(\xi, \eta)]$  independent of the coordinate  $(\xi, \eta)$ , the following relationship applies:

$$S(T) = \int_0^{\infty} N(\lambda, T) \tau_0(\lambda) d\lambda \quad (2-2)$$

where  $N(\lambda, T)$  is the spectral blackbody radiance, and the spectral instrumental transmittance  $\tau_0(\lambda)$  is given by

$$\tau_0(\lambda) = \tau_d(\lambda) \tau_f(\lambda) \quad (2-3)$$

In Eq. (2-1) the value of  $A_d \rho_0^2 / 4F_{eff}^2$  is called instrumental constant  $R_M$ .

For the pyrometer  $A_d = (0.035 \text{ cm})^2$  and for the 155 cm (61 in.) telescope at Agassiz Station:

$$\rho_0 = 0.90 \text{ (at } 10\mu\text{)}$$

$$F_{\text{eff}} = 5.70$$

which gives  $R_M = 0.7636 \times 10^{-5} \text{ cm}^2 \text{sr}$ .

Introducing the above values to Eq. (2-1), we obtain:

$$I_M = 0.7636 \times 10^{-5} \bar{\tau}_A(T, m, \omega) S(T) \text{ watt} \quad (2-4)$$

To evaluate the temperature resolution  $\Delta T(T)$  for a given lunar brightness temperature  $T$ , we obtain from Eq. (2-4)

$$\frac{\Delta I_M}{\Delta T} = 0.7636 \times 10^{-5} \text{ cm}^2 \text{sr} \bar{\tau}_A(T, m, \omega) \frac{\Delta S(T)}{\Delta(T)} \text{ watt}^\circ \text{K}^{-1} \quad (2-5)$$

For the purpose of evaluating Eqs. (2-4) and (2-5), we assume  $\bar{\tau}_A = 0.82$  for  $T = 200^\circ \text{K}$ ,  $m = 1.5$  and  $\omega_0 = 1.4 \text{ mm}$  and the proper values of  $S(T)$  previously calculated; for different temperatures we obtained the values of  $I_M$  and  $\Delta I_M / \Delta T(T)$  given in Table 2-I.

TABLE 2-I

$T(^{\circ}\text{K})$	$S(T), \text{watt cm}^{-2} \text{sr}^{-1}$	$I_M, \text{watt}$	$\Delta I_M / \Delta T(T), \text{watt}^\circ \text{K}^{-1}$
100	$0.412517 \times 10^{-6}$	$2.6 \times 10^{-12}$	$2.5 \times 10^{-12}$
150	$0.292870 \times 10^{-4}$	$1.8 \times 10^{-10}$	$1.1 \times 10^{-11}$
200	$0.275379 \times 10^{-3}$	$1.7 \times 10^{-9}$	$5.8 \times 10^{-11}$
250	$0.109981 \times 10^{-2}$	$6.8 \times 10^{-8}$	$1.5 \times 10^{-10}$
300	$0.282312 \times 10^{-2}$	$1.7 \times 10^{-8}$	$2.8 \times 10^{-10}$
350	$0.560353 \times 10^{-2}$	$3.5 \times 10^{-8}$	$4.1 \times 10^{-10}$
400	$0.945537 \times 10^{-2}$	$5.9 \times 10^{-8}$	$5.4 \times 10^{-10}$

The noise level of the pyrometer has been measured (Section IV, 1) to be  $6 \times 10^{-11}$  watts peak-to-peak for one second time constant. For a given set of lunar measurements (Fig. 4-2a.b.) we used an integration time of 0.2 seconds. Since the noise level is dominantly Johnson noise, the ratio of the noise levels in the two cases will be proportional to  $\sqrt{1/0.2}=2.2$ . Thus, under the same observing conditions and for  $\tau=0.2$  seconds the noise level should be  $1.3 \times 10^{-10}$  watt peak-to-peak. Using the above values and the ones given in Table 2-I, the temperature resolution  $\Delta T(T)$  can be obtained for a given temperature,  $T$ , and the assumed observing conditions. As an example for  $T=150^\circ\text{K}$  a  $\Delta T=10^\circ\text{K}$  could double the peak-to-peak noise level (see Fig. 4-2b.).

### III. RADIATION PYROMETER SYSTEM

#### A. General Description

Figure 3-1 is a block diagram of the radiation pyrometer. The system can be divided as follows:

1. Pyrometer head
2. Electronic console
3. Monitor console .

The pyrometer head houses the detector, preamplifier, its power supply, chopper and its driving mechanism, reference and calibration blackbodies, thermistor sensors and the photographic and visual optical system of the pyrometer. This part of the instrument is attached to the telescope flange.

A set of cables connects the pyrometer head with the electronic console and the monitor console. The electronic console consists of a phase-controlled rectifier, dc vacuum tube voltmeter, different power supplies, and the necessary meters and selector switches. The output of the electronic console is recorded on the paper chart amplifier recorder.

The monitor console consists of a magnetic tape recorder, a digital clock, radio receiver for time signals, an audio-oscillator for event marks, and the intercommunication system between the observer and the operator of the electronic equipment.

Figure 3-2 is a photograph of the actual electronic console, monitor console and paper chart amplifier-recorder.

#### B. Pyrometer Head

A schematic drawing of the pyrometer head is given as Figure 3-3. The head is designed for attachment to the telescope with f-numbers ranging from 3.5 to 6. The beam is intercepted by a glass chopper, C, which is driven by a variable

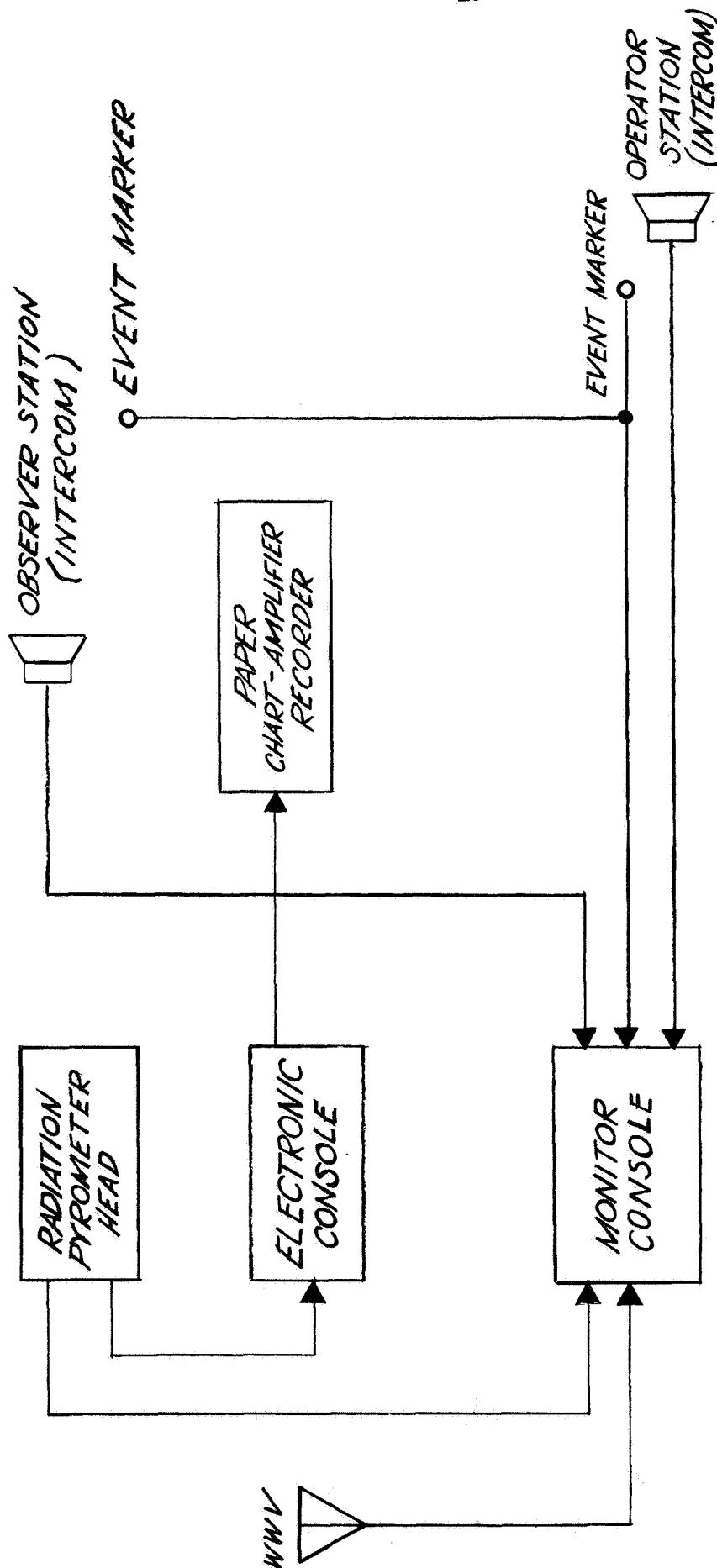


FIG. 3-1. Block diagram of the radiation pyrometer system.



FIG. 3-2. Photograph of the electronic console, monitor console and paper chart recorder of the radiation pyrometer developed at the Harvard College Observatory for lunar observations.

speed drive, G. One side of the chopper is an aluminized surface and the other a gold coated\* surface. Between the chopper blade and the detector system is an entrance stop, S.

For each telescope the entrance stop is chosen to stop down the mirror objective. When the chopper blade uncovers the entrance stop, the detector, D, will receive the infrared signal. By means of the filter slide, F, the proper filter can be selected or the clear or closed positions may be used.

When the chopper is in front of the entrance stop, the detector, D, will exchange radiation with the reference blackbody, B. At the same time, a reflection will take place on the aluminized side of the chopper; the focal plane will be transferred, and it becomes co-planer with the reticle, R. By means of the flat mirror, E, and the camera objective, L, the reticle, R, is imaged on the photographic film. Introducing the diagonal mirror, M, and the pentaprism, P, into the optical path, the observer can see a field of view of  $7!5 \times 5!0$ .

The photographic camera is electrically powered, and can be triggered either by the observer, or by the operator from the electronic console. For each frame that is secured, a signal is recorded on the paper chart and on magnetic tape. Moreover, each signal is counted by an electro-mechanical counter within the electronic console.

When the infrared channel has been refocused after the insertion of an infrared filter, a compensating plate, Q, will be introduced or removed from the path to keep the photographic-visual channel in focus. These compensating plates are operated from the outside of the pyrometer head.

---

\* Gold films have higher spectral reflectance at  $10\mu$  than aluminum films.

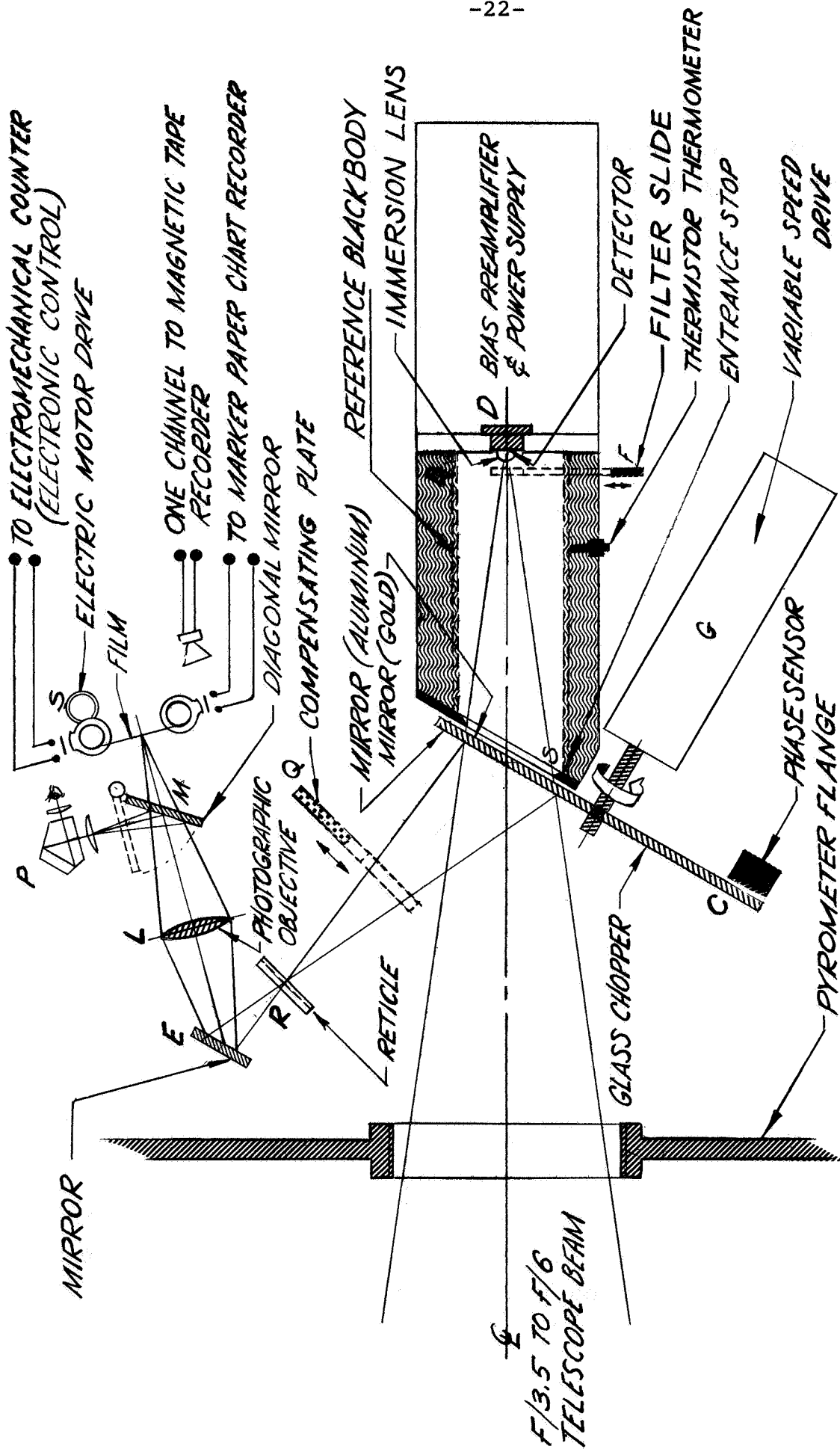


FIG. 3-3. Schematic of the pyrometer head.

Figure 3-4 is a photograph of the inside of the pyrometer head.

#### 1. Variable Speed Chopper Subassembly

Figure 3-5 is an isometric view of the complete variable speed chopper subassembly. This unit is designed to provide a continuously variable speed chopper to set the proper speed in accordance with the time constant of the detector and scanning rates. The unit must also operate as an optical switch for the radiometric and photographic-visual channels. The glass chopper operates as an optical flat for the optical train of the photographic-visual channel. Since we require that the wandering of the image must be kept below  $\pm 1''$ , a special mounting was designed to accurately obtain the perpendicularity of the chopper to its axis of rotation. The unit was designed and built with extreme care in order to:

- a. introduce the minimum amount of vibration to the pyrometer head;
- b. avoid temperature changes on the glass chopper caused by the heat transfer from the motor;
- c. overcome smoothly the inertia of the rotary parts at start and stop;
- d. have constant speed after setting the proper ratio; and
- e. achieve a uniform performance over a range of temperature between  $-20^{\circ}\text{C}$  ( $-40^{\circ}\text{F}$ ) and  $+30^{\circ}\text{C}$  ( $86^{\circ}\text{F}$ ).

##### a. Glass Chopper

As Figure 3-5 indicates, the glass chopper has two blades. It is made of Pyrex 2.4 mm ( $3/32$  in.) thick, and the diameter is 133 mm ( $5\frac{1}{4}$  in.). The surface used in the photographic-visual channel is finished within  $\lambda/4$  wavelength. The side facing the radiometric channel is finished within one wavelength. The chopper was

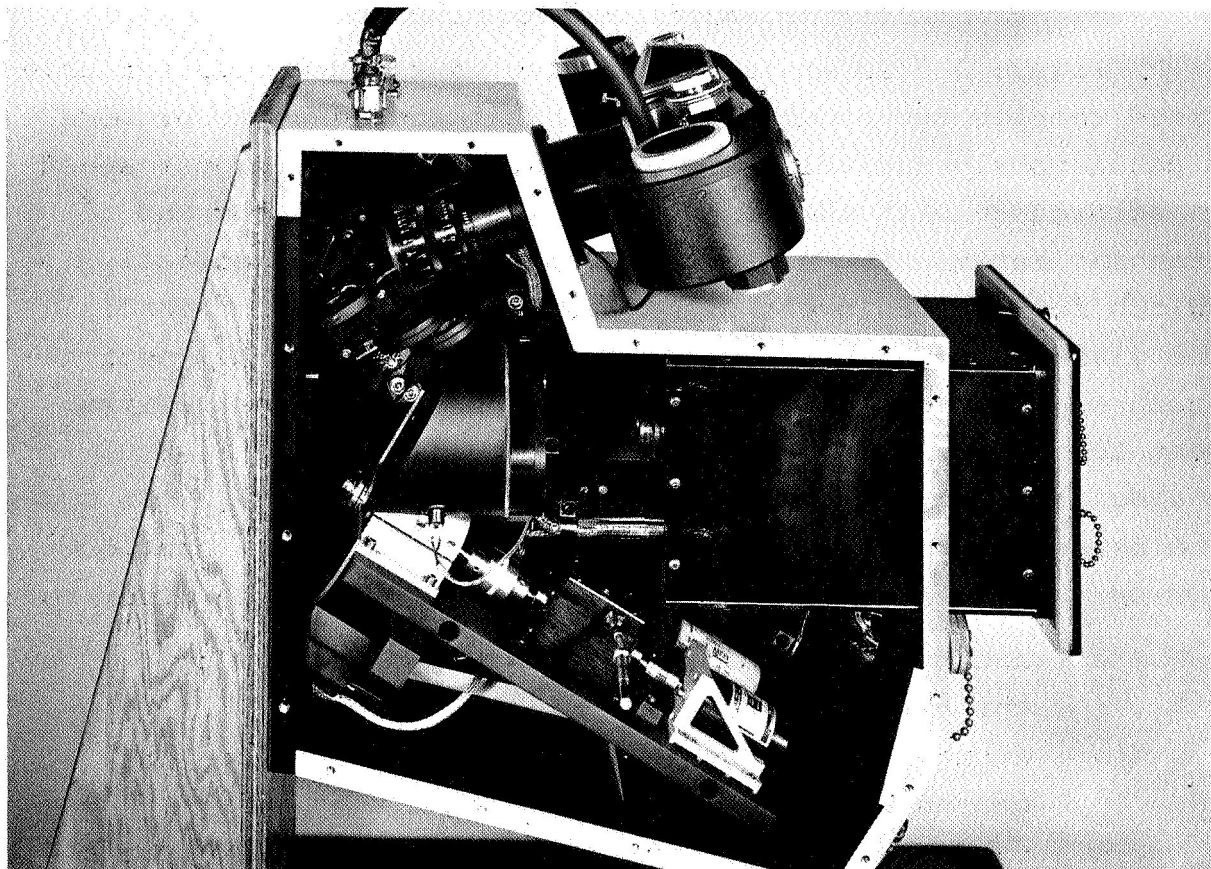


FIG. 3-4. View of the pyrometer head with the side plate removed.

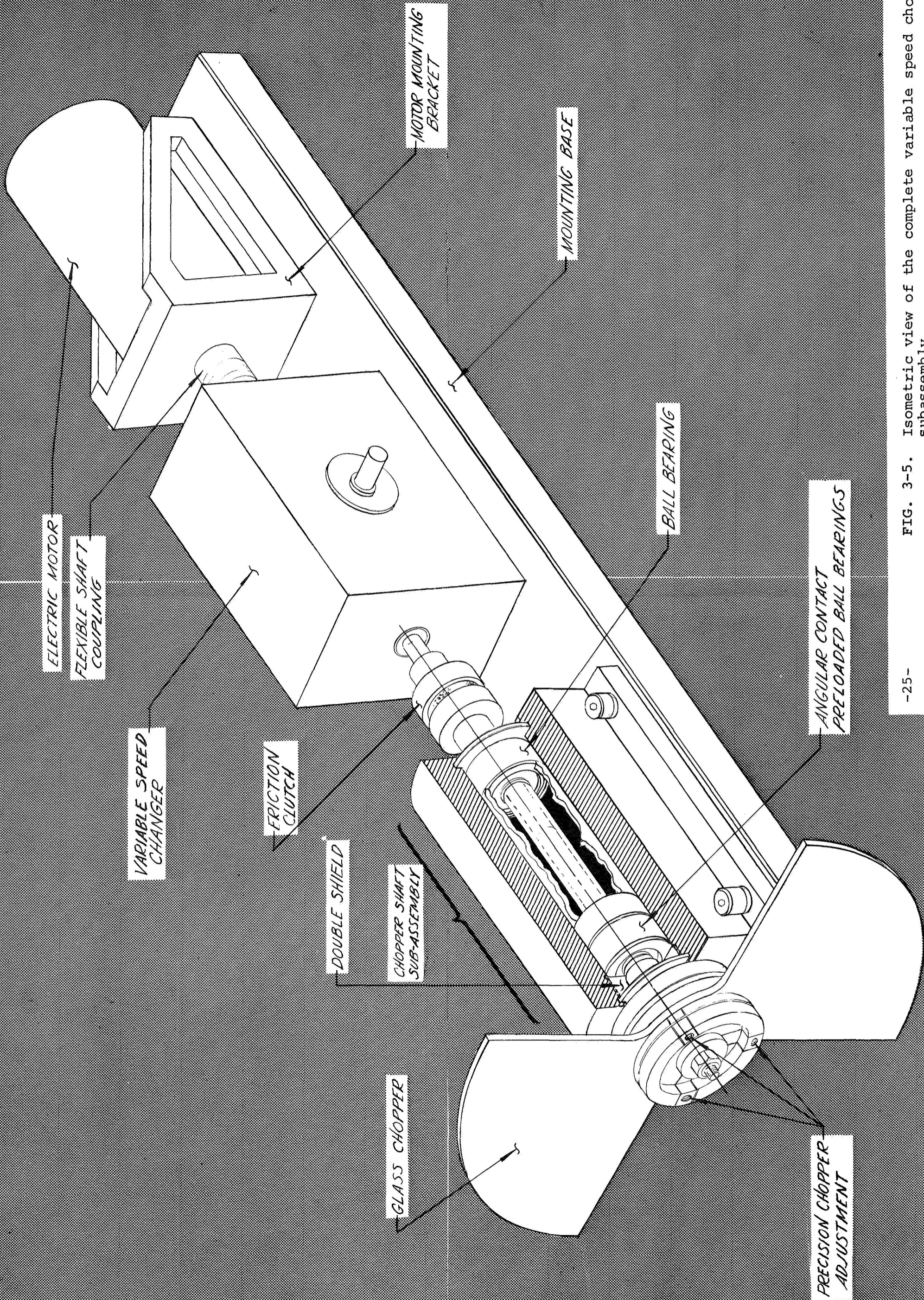


FIG. 3-5. Isometric view of the complete variable speed chopper subassembly.

statically balanced, and the center hole has a good finish for accurate radial centering; the total clearance between the chopper hole and the shaft measure  $20.3\mu$  (0.0008 in.).

Before the chopper was aluminized, it was thoroughly checked. A variation in thickness of the blade of a maximum  $12.7\mu$  (0.0005 in.) was measured with an Etalon Micrometer (0.0001 inch per division). Furthermore, the flatness of the chopper was checked visually, by means of the interference fringe method.

The chopper was coated in our laboratory. The side facing the photographic-visual channel was aluminized. For the other side, gold was evaporated. Since gold does not readily bond to glass, a base layer of Inconel was evaporated first, the gold layer being evaporated on top. To increase the adhesion of the gold, the chopper was baked at  $120^{\circ}\text{C}$  ( $248^{\circ}\text{F}$ ) for fifteen minutes. This method was applied on a sample glass and tests were made, attempting to peel off the coating with masking (Scotch) tape or by scratching it with a needle. Baking definitely improved the resistance to mechanical action on the film.

The chopper holder and adjustment mechanism is indicated in Figure 3-6. The purpose of the adjustment mechanism is to set the chopper perpendicular to the chopper shaft by means of three screws, using an autocollimator as a measuring instrument.

The thickness relationship between the "tongues", A, B and C, as well as the material, was chosen to obtain a non-critical adjustment by means of the screws, D. The surfaces indicated as lapped were finished with Paris rouge to within  $6.3\mu$  (0.00025 in.) on a circle of 25.4 mm (1 in.) diameter.

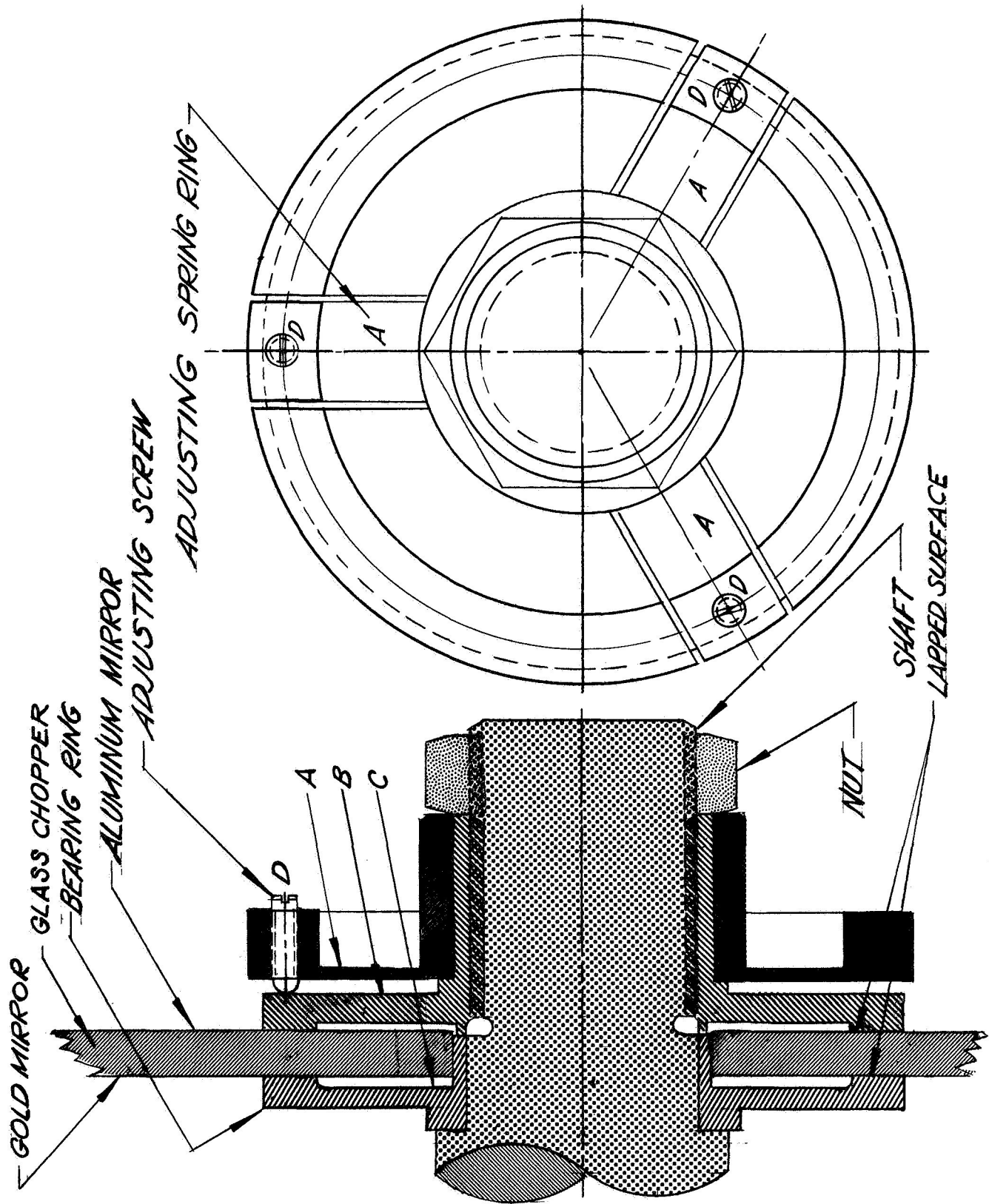


FIG. 3-6. Chopper holder and adjustment mechanism.

b. Chopper Shaft Subassembly

In order to keep the angular adjustment of the chopper precise, and to assure smooth running of the shaft, it was designed as an isostatic system. Two angular contact ball bearings at one end of the shaft eliminates two degrees of freedom, and one ball bearing fitted loosely at the other end of the shaft eliminates the third degree of freedom.

The shaft is made of stainless steel. When finished, it was measured carefully; the off-roundness of the shaft was undetected when using a dial indicator (0.001 in.).

The ball bearings shown in Figure 3-4 are precision type no. 7; the angular contacts are pre-loaded with four pounds. The regular ball bearing has a dust shield as supplied by the manufacturer; the other two angular contact ball bearings\* have a double shielding system designed and fabricated by our group. Looking axially outward from the inside of the bearing, the first stage of the labyrinthine shielding can be seen; the second stage is a cavity filled with medium-viscosity grease. The outside wall of this cavity is a Teflon disk. There is a clearance between the shaft and the disk, but for the range in temperature of  $-15^{\circ}\text{C}$  to  $-25^{\circ}\text{C}$ , ( $+5^{\circ}\text{F}$  to  $+77^{\circ}\text{F}$ ) the surface tension of the grease is enough to avoid any leak through the clearance.

c. Clutch

The friction clutch is provided to allow enough slippage during acceleration or deceleration of the chopper to avoid undesirable dynamic load on the variable ratio speed changer, and to avoid heat transfer from the motor and speed changer to the chopper.

It consists of two aluminum cups with two disks of urethane foam.

---

\* Small sizes of angular contact ball bearings are not supplied with a dust shield by the manufacturers.

d. Variable Ratio Speed Changer

The variable ratio speed changer is commercially available\*. It is a friction-type changer and the ratio range is continuously variable within a 1:5-5:1 ratio. The torque that can be transmitted is from 5-40 inch-ounces, depending on the speed; efficiency is 7 percent.

To change the ratio of the speed changer, the shaft is coupled to a 10-turn counter mounted on the side of the pyrometer head and calibrated in actual chopping frequency.

e. Flexible Shaft Coupling\*\*

The flexible miniature shaft coupling indicated in Figure 3-5 is a precision light-duty type. This coupling is precision machined from one piece of metal made by cutting a helical groove around its outside diameter. The remaining material resembles a knife blade wrapped edgewise around an axial wire. This helical shaft-coupling is laterally flexible and torsionally rigid.

f. Electric Motor

To reduce vibration, we chose an electric motor that operates with a high induction field so that the mass of the rotor is small. The motor indicated in Figure 3-5 is a Globe Industries MC Hysteris Synchronous motor. It has four poles operated from a single-phase, 110 V and 60 Hz power supply, and uses 12 watts. The speed is 1800 rpm, rated at 0.7 inch-ounces. The mounting bracket for the motor has been designed to allow minimum heat transfer by conduction from the motor to the mounting base of the subassembly; cooling is mainly by radiation. At room temperature, the temperature measurement on the motor case was 60°C (140°F); with load, it measured 61°C (142°F)

---

\* Miniature Variable Ratio Speed Changer, Type 2D, Metron Instrument Co., Littleton, Colorado

\*\* Heli-Cal Flexible Shaft-Coupling, Precision Light Duty Series Catalog No. 7-62.

g. Test of the Variable Speed Chopper

The speed range of the subassembly was checked with the chopper mounted. Since at high speed we have limited available torque, the useful range in speed is the one giving a chopping frequency of 10 Hz to 70 Hz.

To detect any possible slippage in the clutch of the variable speed changer, the constancy of the speed was checked electronically (Lissajou's figures). At 10 Hz the deviation in frequency was peak-to-peak  $\pm 0.6$  percent over two hours. Since the motor was connected to the line, we may assume that this variation in frequency came from the power supply line.

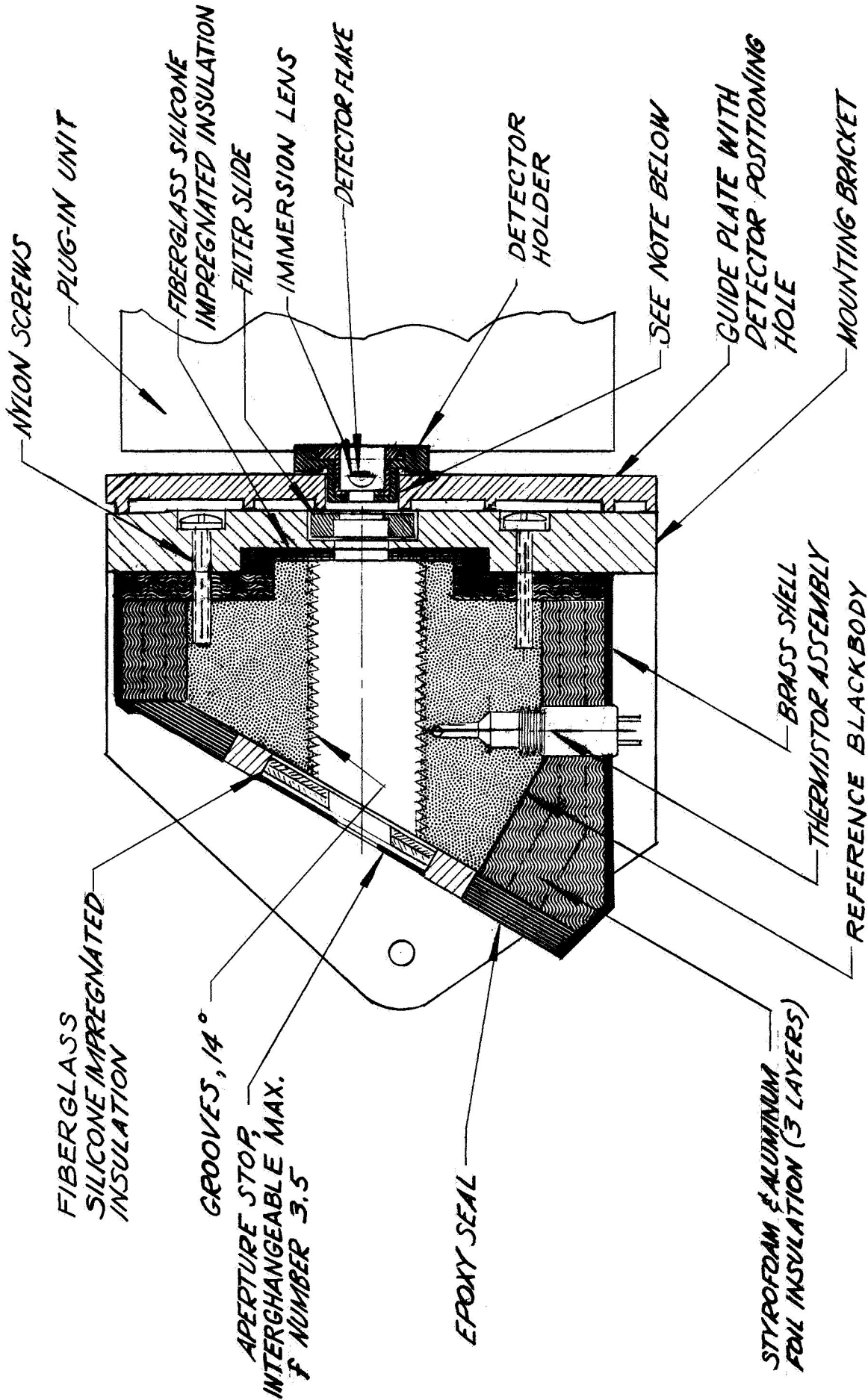
2. Reference Blackbody

The same general considerations that we shall give to the calibration blackbody, (Section III, B-3), apply to the reference blackbody.

This blackbody is shown schematically in Figure 3-7. The basic body is made from cold-rolled steel. The inside has been machined with grooves 3.2 mm (1/8 in.) deep, and a 14° aperture. After machining, it was heated with a torch to oxidize the surface and to obtain higher emissivity.

To reduce gradients in temperature and short-term drift, the body has a substantial thermal capacity. The addition of extremely good thermal insulation all around minimizes heat conduction from or to the rest of the pyrometer head.

As Figure 3-7 shows, the steel core was insulated with alternate layers of closed cell Styrofoam F. B. (Dow Chemical Company) and sheets of aluminum foil in the following sequence, from inside to outside: Styrofoam, aluminum foil, Styrofoam, aluminum foil and Styrofoam. The unit is housed in a brass



NOTE:— CLEARANCE BETWEEN HOLDER AND POSITIONING HOLE  $\pm 0.00025$ "

FIG. 3-7. Schematic of the reference blackbody.

container designed for this application. The front of the reference blackbody has an insulating fiberglass silicone-impregnated ring, and it is sealed all around with epoxy resin. On the fiberglass ring, an aperture stop is mounted which could be replaced in accordance with the f-number of the optical system. The minimum f-number that the blackbody will accept is  $f/3.5$ .

The rear of the steel core is also insulated with a series of Styrofoam and aluminum foil layers.

In order to keep coupling by thermal conduction at a minimum, the reference blackbody is fastened to the mounting bracket by six nylon screws. There is no metal-to-metal contact between the steel core and the rest of the pyrometer head. In addition, the base of the mounting bracket has fins to reduce even more the heat transfer by conduction. The same has been done with the guide plate which positions the detector.

The positioning of the detector is assured by the positioning hole, as Figure 3-7 shows. The clearance between the detector mount and the hole is  $\pm 0.00025$  inches.

Previous experience has shown that it is not advisable to have a controller for the temperature of the blackbody. Instead, it is more reliable to monitor the temperature continuously, and to record the temperature at the time of the measurements (provided that the measurements last for a short time, as compared to the thermal time constant of the calibration blackbody). To measure the temperature, we used a bead thermistor (Section III, B-4).

Figure 3-8 shows photographs of the reference blackbody before the insulating layers had been put on: (a) taken from the guide plate side, and (b) taken from the aperture stop side.

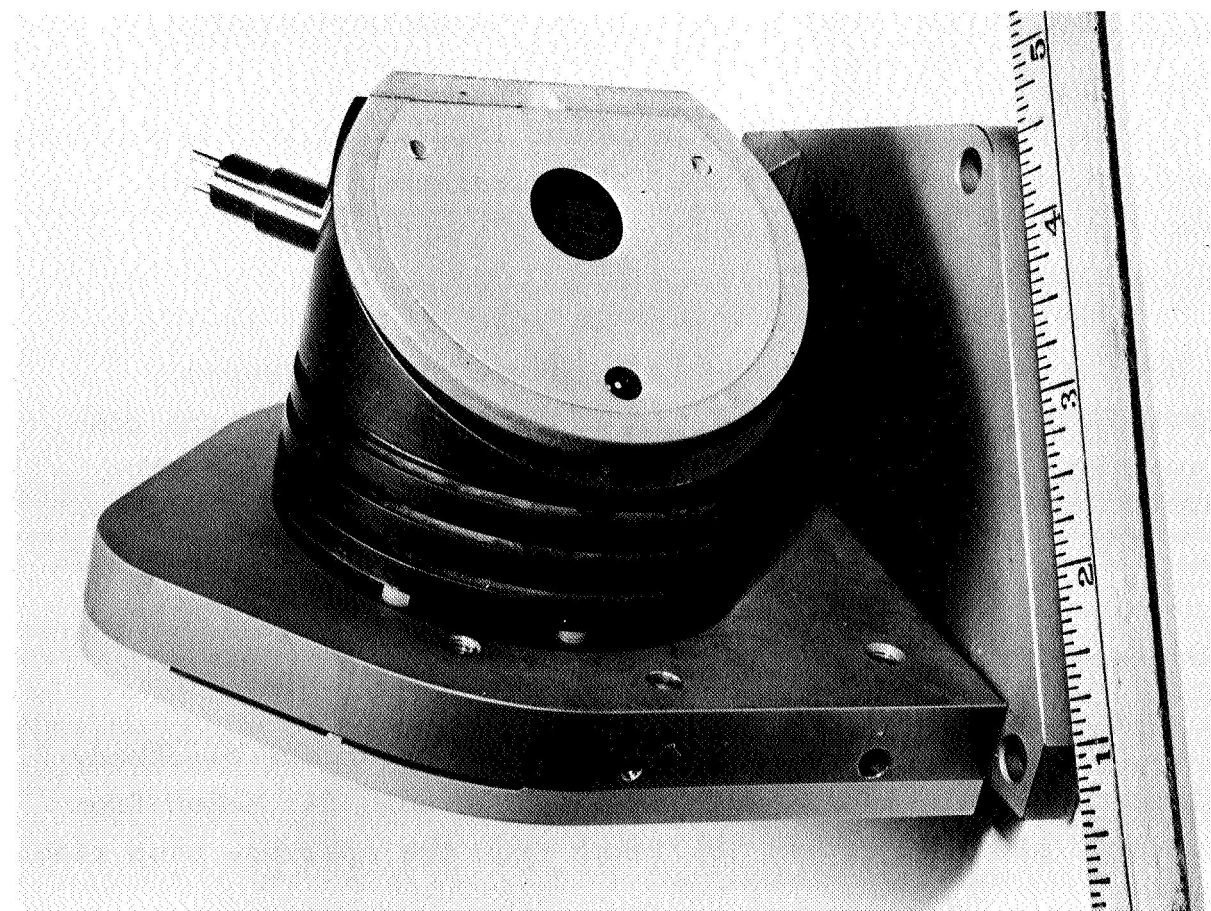
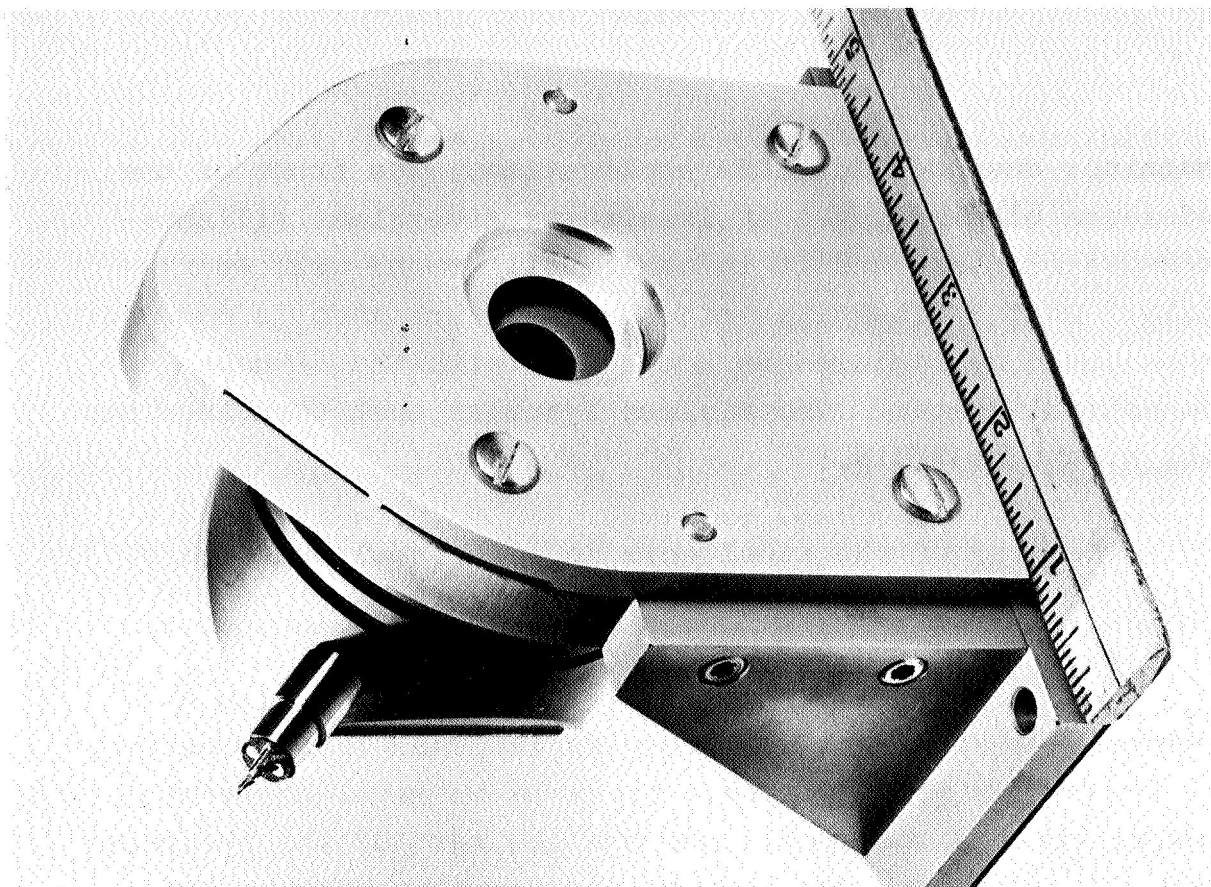


FIG. 3-8. Views of the reference blackbody before insulation;  
a.) from the guide plate side, b.) from the aperture  
stop side.

### 3. Calibration Blackbody

For the calibration of the pyrometer at the telescope we used a blackbody (Figure 3-9) that is heated by heating element and the temperature is measured using a thermistor thermometer.

Several problems became apparent in the design of such a blackbody:

1. Any conventional blackbody cavity, such as conical, cylindrical-conical, double-reversed conical, etc., becomes prohibitively large when a big opening is required.
2. Gradients of temperature occur on the cavity itself unless extreme care is taken.
3. Errors arise in the temperature reading of the blackbody.
4. The value of the effective emissivity is not known.

The solution to problem 1 is to use a Fresnel-type of blackbody<sup>5</sup>. Because of difficulties in machining of the 14° grooves, we switched to parallel wedges with 15° angle<sup>6</sup>. The choice of material for the blackbody should be made on the basis of its thermal diffusivity, maximum thermal capacity, and high emissivity. The most practical materials to analyze will be copper and steel. Table 3-I gives the thermal diffusivity, ratio of thermal capacities for unit volume and emissivities. Table 3-I shows that because of its high diffusivity copper is less susceptible to thermal gradients than steel. There is practically no difference in thermal capacity of copper, but its emissivity is appreciably lower than steel. Probably, emissivity can be increased by chemical etching of the surface.

In our case, steel rather than copper was chosen mainly on the basis of higher emissivity. To reduce the probable gradients, the blackbody was very well insulated.

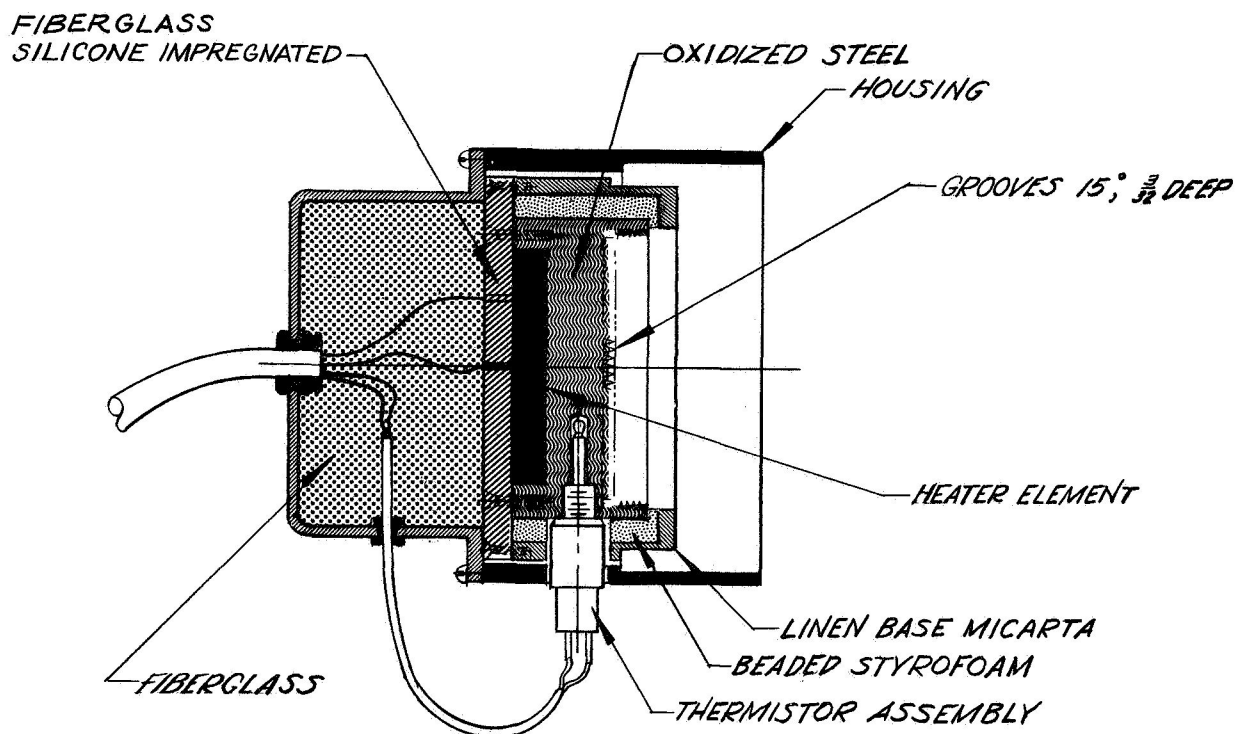


FIG. 3-9. Schematic of the calibration blackbody.

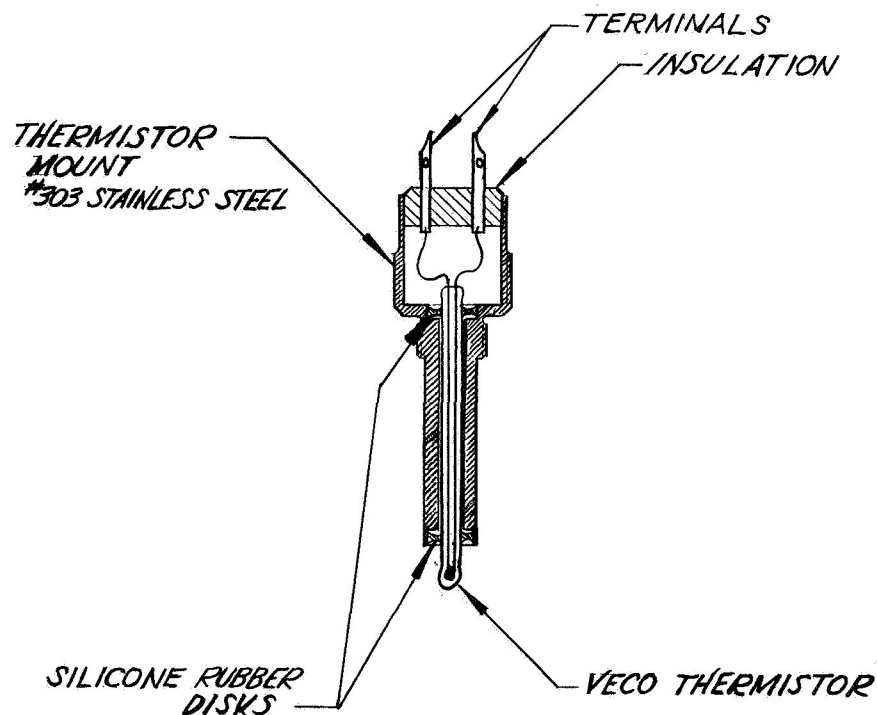


FIG. 3-10. Cross-section of the thermistor assembly units.

TABLE 3-I

Material	Thermal Diffusivity <sup>*</sup> $\text{cm}^2 \text{s}^{-1}$	(Thermal Capacity) copper <hr/> (Thermal Capacity) steel	Radiant Emissivity <sup>*</sup>
Copper	1.2	1.0	at 200 C (Oxidized), 0.6
Steel	0.128	1.1	at 200 C (Oxidized), 0.79 at 25 C, 0.80

\* Data from Handbook of Chemistry and Physics, Edition 1957-58.

#### 4. Thermistors

The sensing elements for measuring the temperature of the reference and the calibration blackbody are hermetically-sealed bead thermistors manufactured by Victory Engineering Corporation. For the reference blackbody, we used a thermistor, Model 32A38B2, which has a resistance of approximately 2,000 ohms at 25°C (77°F) with a temperature coefficient of -3.9% per °C (-2.2% per °F). For the calibration blackbody we used Model 33A7S1, which has a resistance of approximately 5,000 ohms at 25°C (77°F) with the same temperature coefficient.

Each thermistor was mounted in a holder in accordance with the schematic diagram given in Figure 3-10. Three main considerations led to this design:

1. Easy substitution in the case of failure of the thermistor, or a change in its calibration;
2. protection of the glass envelope of the thermistor; and,
3. good thermal coupling between the bead and the blackbody.

The glass thermistor is mounted in a stainless steel holder and is held at both ends by means of two silicone rubber disks. This arrangement has the distinct advantage of allowing good thermal coupling between the bead thermistor and the blackbody. Moreover, because of the silicone rubber mounting, a light pressure by the bead on the blackbody can be achieved. In the final assembly, a drop of Dow-Corning Heat Sink Compound No. 340 is placed on the tip of the thermistor glass envelope to increase the effective thermal coupling between the thermistors and the blackbodies.

#### 5. Optical Filters

##### a. Infrared

On the basis of the solar spectral radiant emittance, the range of temperatures expected on the moon, and the spectral

transmittance of the atmosphere, we used the  $8\mu$  to  $14\mu$  region for our measurements. In this region, several absorption bands exist due to  $O_3$ ,  $H_2O$ ,  $CO_2$  and  $N_2O$ . The existence of these bands makes the determination of the atmospheric attenuation a rather complicated affair when carrying out absolute measurements. If the properties of the atmosphere remain the same, relative measurements simplify the problem considerably.

Because of this, we chose a set of two filters, one for relative measurements and another for absolute measurements. Figure 3-11 gives the spectral transmittance of the filter for absolute measurements, (curve 2), and for relative measurements, (curve 1), as well as the spectral transmittance of the earth's atmosphere, where the strong atmospheric bands are indicated. The spectral transmittance given by curve 1 is obtained by a long wave pass filter with a Ge substrate .040 inches thick and a  $BaF_2$  blocking window. The bandpass interference filter, which gives the spectral transmittance given by curve 2 was obtained by the deposition of a series of about fifty dielectric and semiconductor layers on Itran II substrate.

These filters were checked by the manufacturer for operation at lower temperatures and different angles of incidence. The filters were checked periodically with a Perkin-Elmer spectrophotometer. Our experience with interference filters indicated that moisture could get between the evaporated layers and completely modify the transmittance of the filters. This is particularly noticeable if care has not been taken to seal around the edge of the filters properly. We did not have moisture problems with the substrates for Itran II ( $ZnS$ ) and Ge; these were given a solubility of  $0_{gr}/100ml$  of  $H_2O$  at  $20^\circ C$  ( $68^\circ F$ ). The  $BaF_2$  blocking window had a solubility of only 0.17 under the same test conditions, and is slightly hygroscopic.

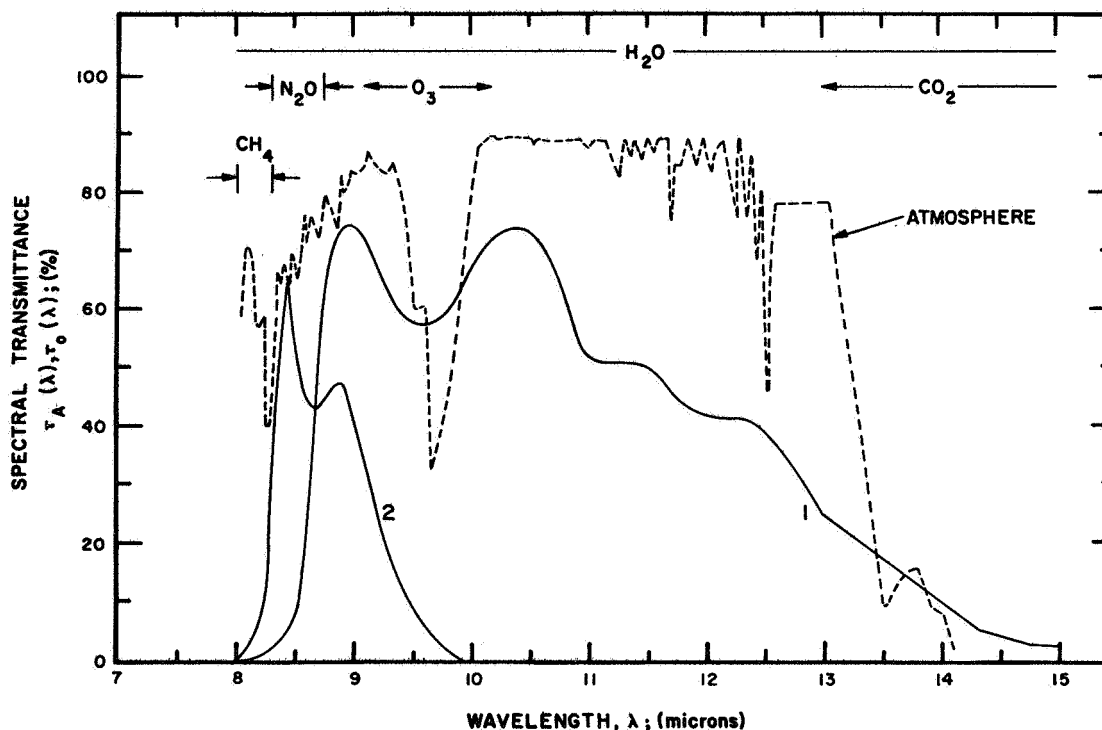


FIG. 3-11. Spectral transmittances  $\tau_o(\lambda)$  of 1) wide-bandpass filter detector window combination, and 2) narrow-bandpass filter detector window combination. Predicted spectral atmospheric transmittance  $\tau_A(\lambda)$  based upon our model for 10 mm of precipitable water and  $m=1$ . Regions of the spectrum with the important absorbing constituents are marked. (The region between  $12.54$  and  $13.0\mu$  has been interpolated.)

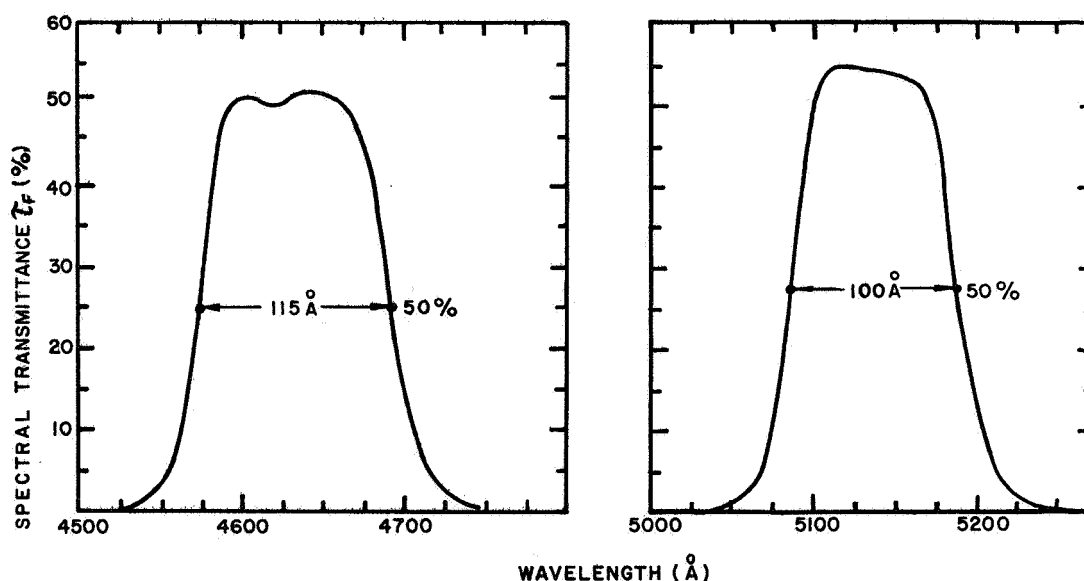


FIG. 3-12. Spectral radiant transmittance of the two multilayer interference filters for the visible channel of the radiation pyrometer.

To minimize all the moisture problems, the filter slide which holds the filters is removed from the pyrometer head when the instrument is not in use, and is kept in a box with silica gel.

b. Visible

The filters in the visible range were multilayer interference filters. The actual spectral transmittance is given in Figure 3-12. One filter was centered at  $4362 \text{ \AA}$  and had a bandpass of  $115 \text{ \AA}$ ; the second one was centered at  $5135 \text{ \AA}$ , with a  $100 \text{ \AA}$  bandpass. At present the two filters are mounted in the slide holder.

Both Grainger<sup>7</sup> and Coyne<sup>8</sup> have reported lunar luminescence in the  $5000 \text{ \AA}$  to  $5300 \text{ \AA}$  band, but Grainger reports an absence of luminescence between  $4500 \text{ \AA}$  and  $4800 \text{ \AA}$ . At these wavelengths the difference in brightness between maria and mountainous regions on the moon is less than toward the red part of the spectrum.

6. Focusing Compensator

Once the infrared detector is focused, we should also keep the visual-photographic channel focused. This adjustment is done once at the laboratory. During actual observing conditions, we have to reset the focusing of the infrared channel in accordance with the filter that is inserted in the optical path. Since we have a given set of filters in the filter holder, we can obtain the optical thickness of each filter with accuracy, and introduce or remove a compensating plate in the visual-photographic channel (see Figure 3-13). Furthermore, we have to maintain the perpendicularity to the optical axis of both the infrared filter and focusing compensator to assure that the homologous points move along the optical axis, and do not suffer any angular displacement which would introduce an inadmissible error into the location of the resolution element.

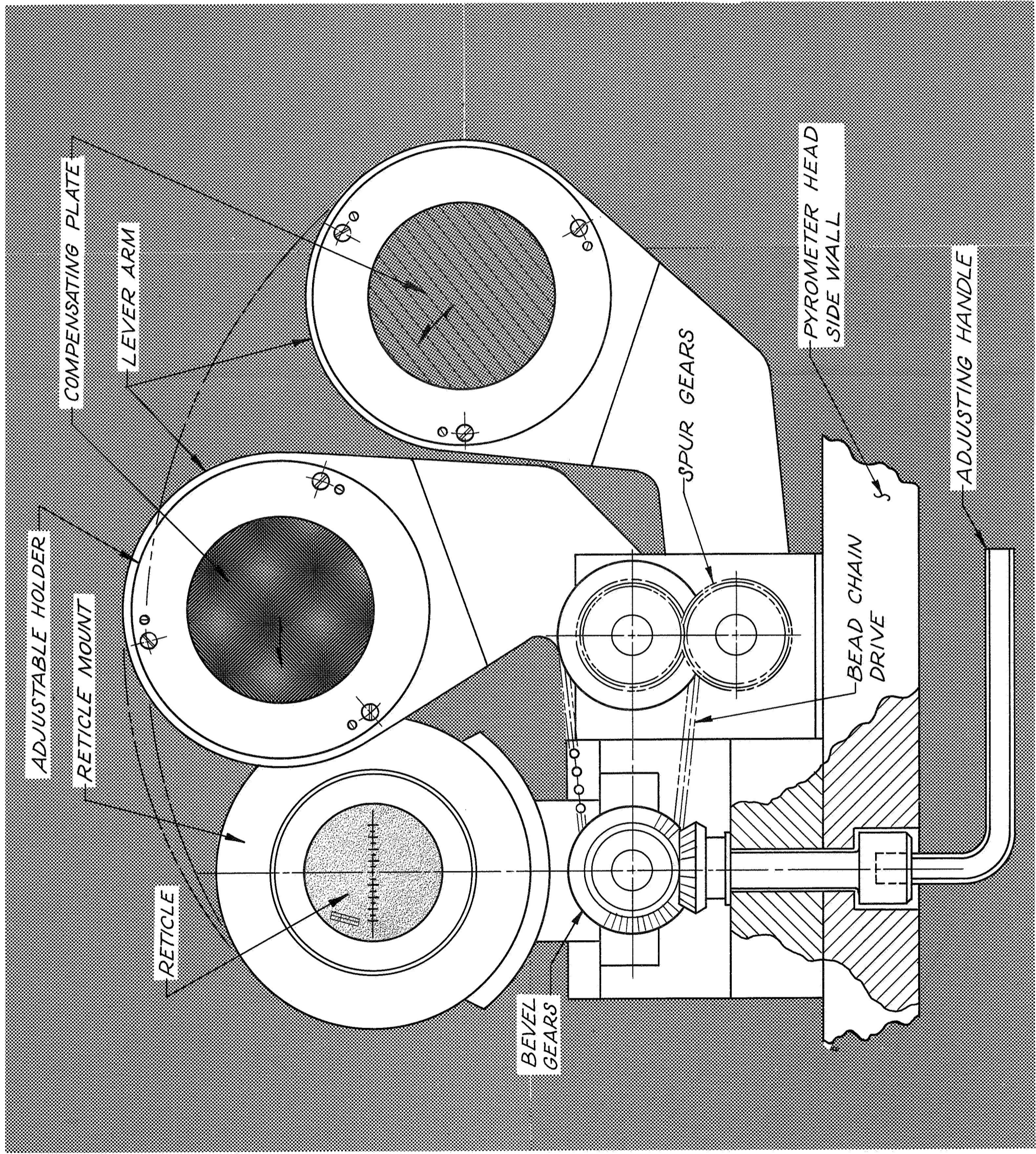


FIG. 3-13. Focusing compensator mechanism.

Figure 3-14a. shows the detector flake immersed in a germanium hemispheric lens. Figure 3-14b. shows the ray tracing before and after the filter has been introduced into the path of the rays.

If we consider that the filter is not perpendicular to the optical axis and is tilted by an amount  $\Delta\theta$ , the point A' will suffer a displacement  $\Delta r$  expressed by:

$$\Delta r = \frac{H}{\cos^2 \theta} \Delta \theta \quad , \quad (3-1)$$

where  $\theta$  is the angle of incidence on the filter, and H is the distance from the rear surface of the filter to the focal point.

If we take as a tolerance  $\Delta r \leq \pm 0.01$  mm for our equipment,  $\Delta\theta = \pm 2'$ .

The same consideration of perpendicularity to the optical axis of the infrared filter applies also to the compensating plates. In this case, H will be the distance from the compensating plate to the reticle, and is 40.5 mm (1.59 in.) for the plate furthest away from the reticle. If we assume that because of the introduction of the plate we can tolerate a maximum error of  $\Delta r \approx \pm 0.05$  mm on the reticle, the maximum angular error that can be tolerated is  $\Delta\alpha \approx \pm 4'$ .

The displacement of  $\Delta f$  from A to A', when a filter of thickness d and index of refraction n is introduced perpendicular to the optical axis, is given by the following expression:

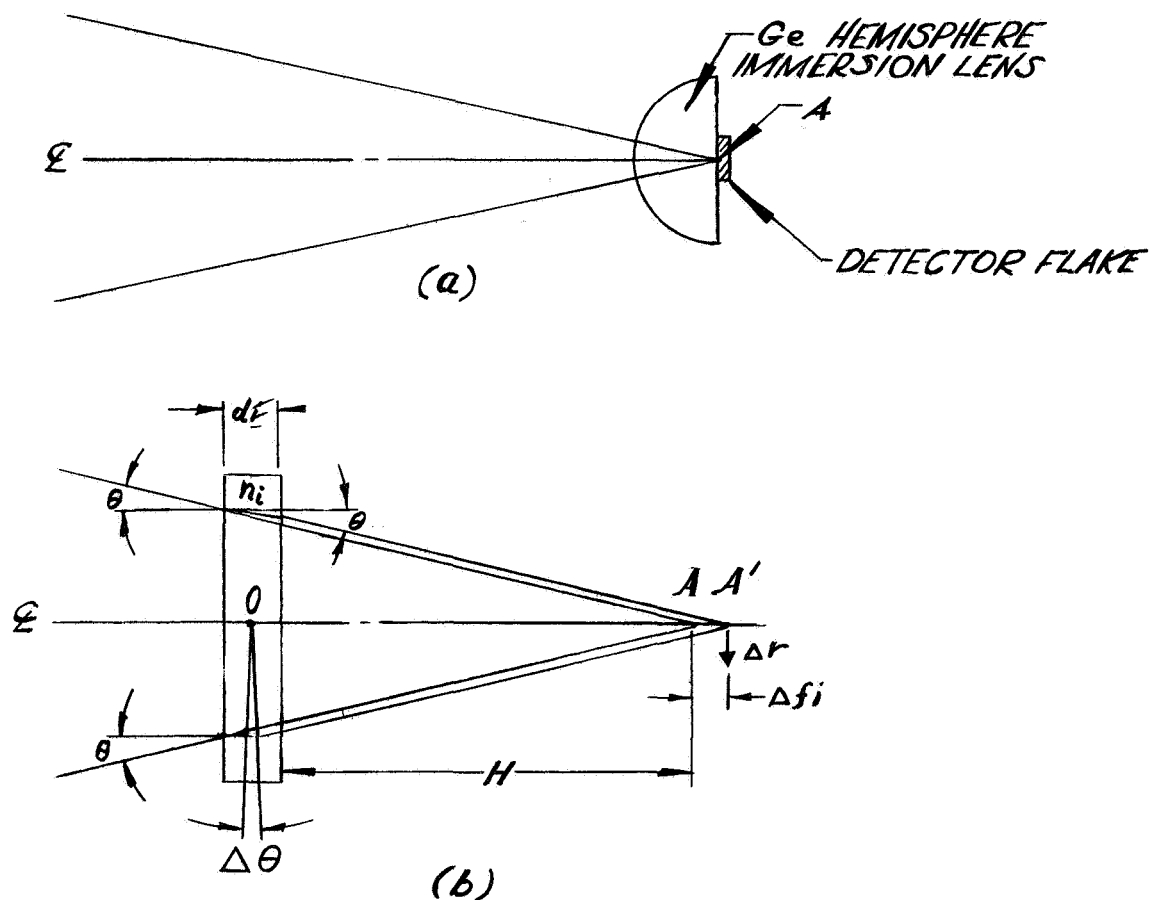


FIG. 3-14. Effect in the focusing produced by the insertion of filters or compensating plates in the optical path; a.) immersion lens, b.) filter or compensating plate.

$$\Delta f = d \frac{\sqrt{n^2 - \sin^2 \theta} - \cos \theta}{\sqrt{n^2 - \sin^2 \theta}} \quad (3-2)$$

For an optical system with an f-number  $f/5$ , we can rewrite Eq. (3-2):

$$\Delta f = d \frac{n - 1}{n} \quad (3-3)$$

An additional blocking filter might be added with other optical and dimensional characteristics than the substrate of the interference filter. In this case, Eq. (3-3) will become:

$$\Delta f = \sum_m d_m \frac{n_m - 1}{n_m} \quad (3-4)$$

where  $m$  is the number of optical media along the path.

Introducing the proper values for Filters No. 1 and 2 (spectral transmittance given in Figure 3-11) into Eq. (3-4) we obtain:

$$\begin{aligned} \text{Filter No. 1 } \Delta f_1 &= +1.5 \text{ mm} \\ \text{Filter No. 2 } \Delta f_2 &= +0.56 \text{ mm} \end{aligned}$$

On the basis of the changes in focus  $\Delta f_1$  and  $\Delta f_2$ , we computed the thickness of the focusing compensating plates manufactured from glass with an index of refraction  $n_D = 1.65 \pm 0.02$ . The thicknesses are  $d_1 = 3.93 \text{ mm}$  and  $d_2 = 1.41 \text{ mm}$ , respectively. Both sides of these plates have an anti-reflection

coating. Each compensating plate is mounted on a lever mechanism which can be operated from outside the pyrometer head by means of a handle.

#### 7. Reticle

The reticle is a crossline-type with the horizontal line graduated in 1/2 millimeters. The reticle is engraved on glass 21 mm (0.827 in.) in diameter and 3 mm (0.118 in.) thick. The illumination is from the side, by means of two grains of wheat bulbs (Chicago Miniature Lamp Works No. CM 8-666); the brightness is controlled by means of a rheostat at the electronic console.

The reticle is on a mounting with the proper adjustment screws for optical alignment.

#### 8. Photographic Camera

The photographic camera is a 35 mm Nikon F. It is a reflex camera with pentaprism. We mounted a Nikon objective f/2.0 which has 50 mm focal length. The capacity of the cassette is 9.1 meters (30 ft.), equivalent to 250 exposures. The field of view of the camera is 7!5 x 5!0 when a telescope with a scale of 25"/mm is used; this field size allows a proper area identification over any region of the lunar disk.

The film transport is driven by a 12 V dc motor and can be triggered by push-buttons on the pyrometer head or from the electronics console.

Every time a picture is taken, a signal is recorded in the event channel of the paper chart recorder; an audio signal is made on the magnetic tape recorder; and, also, each exposure is counted by an electromagnetic counter in the electronic console and in the head.

To prevent loss of data caused by the depletion of the film supply, we added a switch and a circuit to the interior of the camera, with an external bulb to indicate when the entire roll of film has been used; the bulb lights when only one frame is available.

The range of exposure time is from 1 second to 1/1000 seconds. Moreover, for lunar photography, we need Kodak Plus X film. This is a three-layer film designed for use where light conditions during the exposure are unpredictable and the range in image brightness is much larger than the dynamic range of a standard film.

To determine the minimum temperature at which the camera could operate, we ran a test in an environmental chamber for low temperatures. The camera was operated for a long period of time without failure down to  $-22^{\circ}\text{C}$  ( $-7.6^{\circ}\text{F}$ ).

## 9. Phase Sensor

The phase sensor, H, indicated in Figure 3-3, is a reflection-type sensor and consists of an aluminum block which holds a subminiature Ge photodiode (Amperex OAP12) and a light bulb with a condensing lens (GE-224). These two components are mounted in bores at a  $60^{\circ}$  angle. When the glass chopper is in front of the phase sensor, the light beam from the bulb is reflected on the mirror and falls on the photodiode. The clearance between the chopper and phase sensor is 1.6 mm (0.063 in.). The output from the phase sensor is a square wave with very small rise time. Moreover, since the photodiode works at the point of saturation, any small changes in the bulb brightness do not change the amplitude of the square wave. The whole phase sensor subassembly could be adjusted over an angular range of  $76^{\circ}$  to get the proper electrical phase with the output signal from the preamplifier.

## 10. Plug-In Units

Different detectors with the associated electronics as well as focusing mechanism have been built in the form of interchangeable plug-in units for use in connection with the radiation pyrometer head.

At present the pyrometer has the following plug-in units:

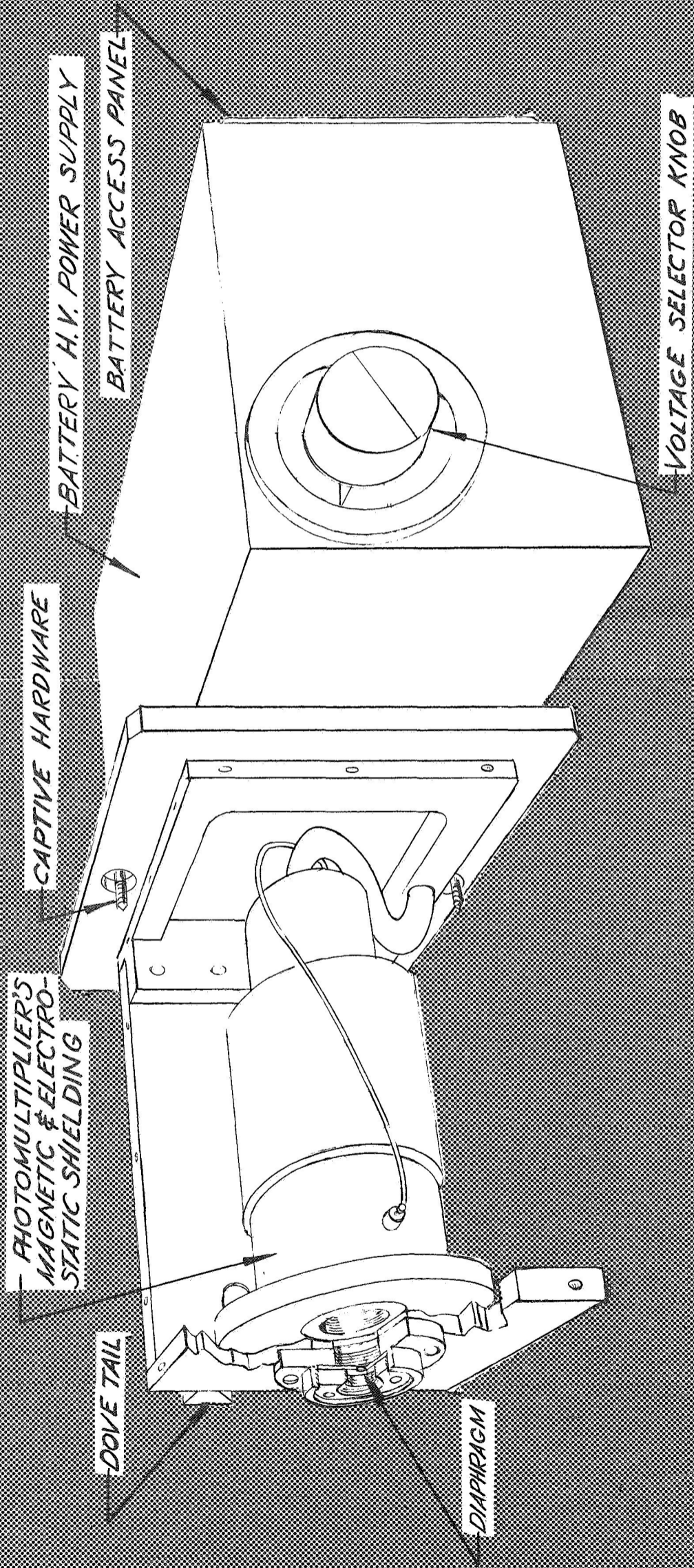
- a. For measurements in the visible range with an EMI-9524B photomultiplier tube including the power supply;
- b. for focusing purposes using the Foucault test as principle; and,
- c. for measurements in the infrared range with the BE-2861 (see Table 3-II) immersed thermistor bolometer including bias supply preamplifier, power supply and switches.

### a. Visible

This unit will allow the visual scanning of the same areas of the moon that have been measured thermally. The photoelectric channel will subtend approximately the same field of view. The exit stop is a circular diaphragm 0.33 mm (0.013 in.) in diameter.

This plug-in unit (see Figure 3-15) consists of a photomultiplier tube EMI 9524B with  $S_{11}$  spectral response, a high voltage power supply made of mercury batteries (Mallory Type RM-413).

The gain of the photomultiplier tube could be adjusted to include only part of the secondary stages because of the large dynamic range in lunar brightness under which the tube must operate.



The batteries were potted in epoxy, and the photomultiplier tube was provided with an excellent magnetic and electrostatic shielding.

The output of the photomultiplier has been loaded with a 1 megohm resistor and has been coupled to the phase-controlled rectifier by a 10 $\mu$ f x 150 V non-polarized tantalum capacitor.

b. Focusing and Foucault Test

Focusing a large telescope with an infrared radiometer attached can be very troublesome. This is particularly true if the focal plane lies in an inaccessible location deep within the instrument enclosure. Moreover, the insertion of filters that are opaque to visible radiation makes the focusing of the instrument even more difficult. Temperature changes during the course of a night, flexure in the telescope, and other less obvious causes may change the relative position of the focal plane of a large telescope. If an instrument is to be used for making measurements with high spatial resolution, the technique for focusing must be made convenient so that the focus may be checked at frequent intervals throughout the course of the observing.

The focusing of the telescope with which the pyrometer is used, is achieved by means of a Foucault test.

The preamplifier-detector plug-in unit is removed from the back of the pyrometer and replaced by the Foucault test plug-in unit. Figure 3-16 shows the ray tracing of the system.

The optical system consists of the knife-edge and two projection lenses, a 75 mm f/2.5 Minolta Rokkor and a 38 mm f/7.6 Simpson 16 mm projection lens. When the telescope is in focus, a real image will lie in the plane of the knife-edge,

APERTURE OF THE ENTERING BUNDLE  $f/5$   
 MAXIMUM APERTURE OF THE ENTERING BUNDLE (TELESCOPE APERTURE)  $\approx f/3$

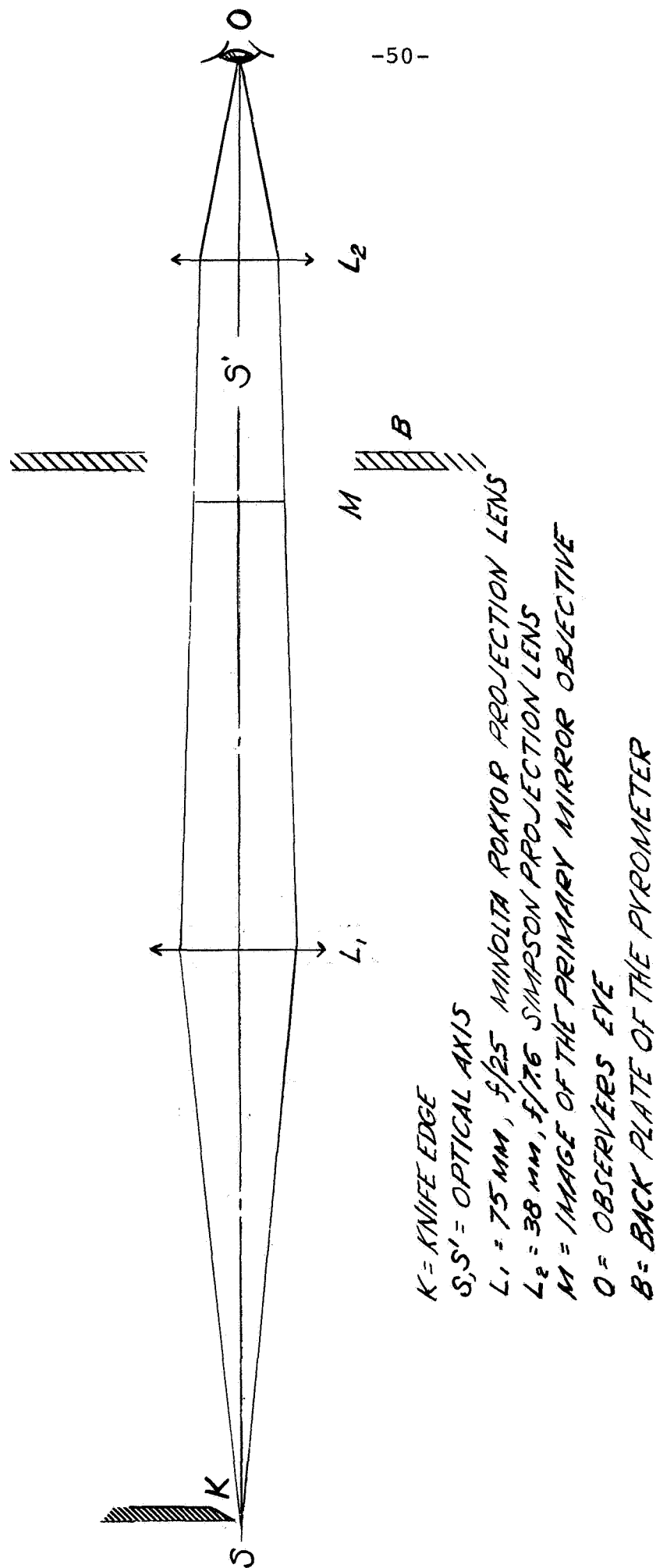


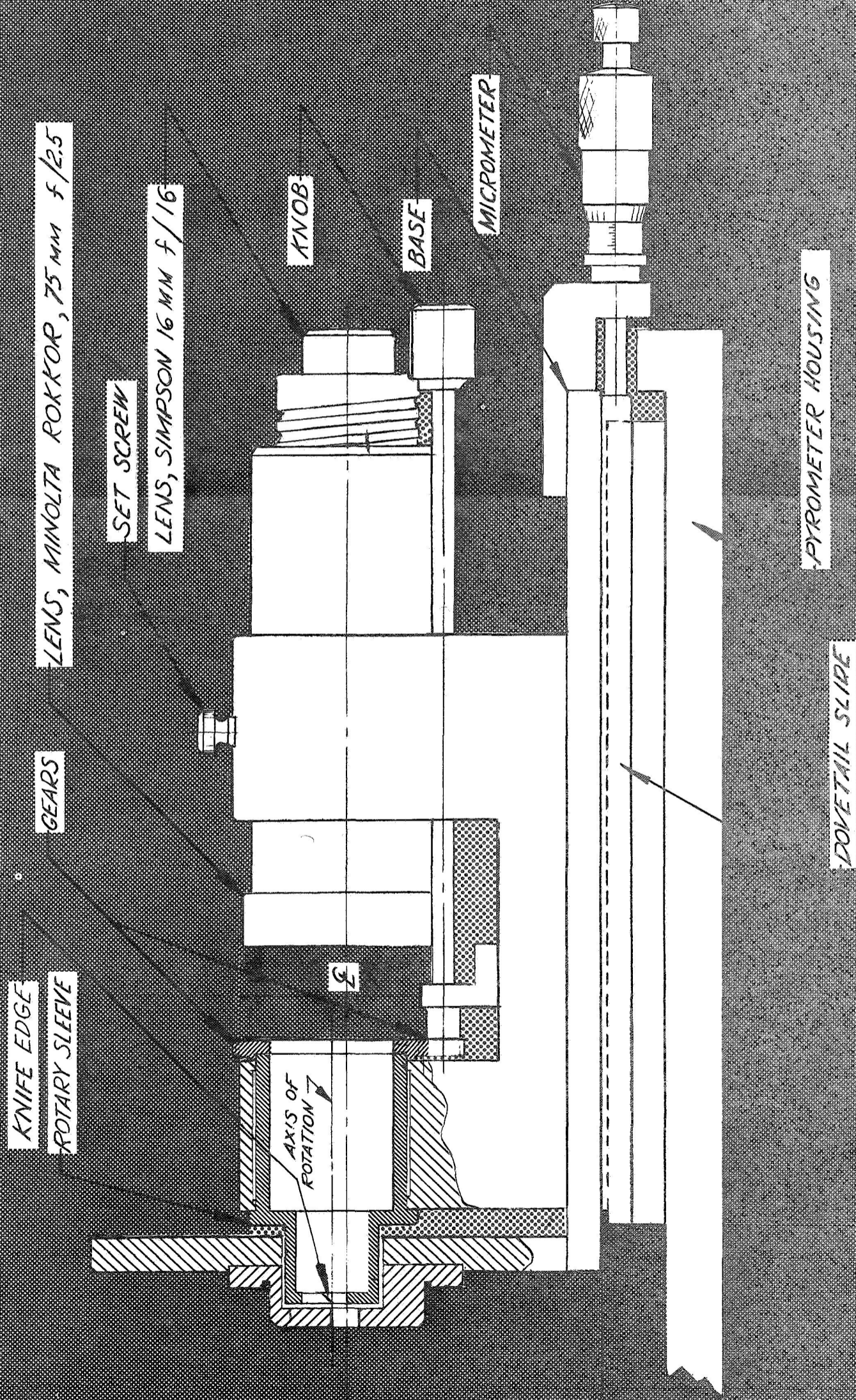
FIG. 3-16. Ray tracing for the Foucault test plug-in unit.

k . Lens  $L$ , the Minolta Rokkor, forms a real image of the primary mirror at  $M$ , and this image can then be examined by the observer's eye at  $O$  with the aide of the Simpson projection lens,  $L_2$ .

Figure 3-17 shows the mechanical arrangement of the Foucault test plug-in unit. The knife is mounted in one end of a sleeve. The sleeve can be rotated about an axis parallel to the optical axis of the unit, but not coincident with it. A gear is attached to the sleeve, and a smaller gear meshes with it. The small gear may be rotated by turning its mounting shaft, and it, in turn, rotates the larger gear, the sleeve and knife-edge. Because of the eccentric mounting of the sleeve relative to the optical axis of the tester, rotation of the sleeve makes the knife-edge move back and forth across the axis. This rotary device replaces the more complicated mechanism usually employed in Foucault testers.

When the pyrometer is to be used, the preamplifier-detector plug-in unit is slid into the instrument until one of the front surfaces of the detector mount is in contact with the rear surface of the guide plate (see Figure 3-8b.). Since the reference body is in a fixed position in the pyrometer housing and since the position of the thermistor detector is fixed relative to the guide plate, the placing of these two surfaces in contact determines the position of the detector in the pyrometer. The position of the detector in its mount is known from the manufacturer's specifications.

When the telescope is to be focused with the Foucault unit there must be some means of positioning the knife-edge in the same plane as that in which the detector lies when it is in the pyrometer. This is accomplished in the following manner:



The position of the knife-edge relative to the front surface of the Foucault unit is known from measurements in the laboratory. Since the position of the detector relative to the rear surface of the reference body is known, the separation between the rear surface of the reference body and the front surface of the tester which will make the knife-edge and the detector lie in the same plane may be calculated. In the laboratory, a feeler gauge of this calculated thickness is placed in contact with the rear surface of the reference blackbody and the Foucault tester is slid into the pyrometer until its front surface makes contact with the feeler gauge. The knife-edge will then lie in the plane which the detector occupies when it is in the pyrometer. The micrometer thimble is then turned until the spindle bears against a plate fixed to the pyrometer housing. The reading of the micrometer is recorded.

To focus the telescope during a night of observing, the preamplifier-detector plug-in unit is removed from the pyrometer, the micrometer on the Foucault tester is set to the previously recorded setting, and the unit is slipped into the pyrometer until the micrometer spindle bears against the plate attached to the housing. The knife-edge is then viewed while being rotated slowly, and the telescope focus is racked back and forth until the best focus is found.

The tester is then removed, and the preamplifier-detector unit is replaced. The entire focusing operation, including the changing of plug-in units, takes only a few minutes and has been found to be completely satisfactory.

### c. Infrared

For the infrared channel two plug-in units have been designed and built; of the two only one will be described in this report since only one will be used to gather lunar data.

### c.1 Thermistor Bolometers

Since the theory and operation of thermistor bolometers is well covered in the literature<sup>9,10,11</sup> we therefore refer only to the characteristics which are more relevant to the operation at the telescope. The thermistor bolometer used in our pyrometer is manufactured by the Barnes Engineering Co., Stamford, Connecticut. By means of plug-in units, developed under the grant, we have the option to use either a regular thermistor or an immersed one. The relevant characteristics of both bolometers are given in Table 3-II.

The thermal coefficient of the thermistor is of the order of -4% per °C.

The resistance of a thermistor obeys a simple exponential law:

$$R = K e^{\beta/T} \quad , \quad (3-5)$$

where R is the resistance, K is a constant determined by the specific resistance and geometry of the element, and  $\beta$  is the constant for each material. For the material of our thermistor  $\beta = 3400^\circ\text{K}$ .

At 25°C (77°F) our thermistor has a resistance  $R = 2.49$  megohm. Using the values given above and using Eq.(3-5), we obtain  $K = 27.63$  ohm.

We expect the pyrometer to operate at temperature as low as -15°C (5°F) and as high as 20°C (68°F). At the extreme high temperature we can assume an increase of 5°C (9°F) inside the radiometer due to the heating of the electronic components.

If we consider the steady state operation of the thermistor, the Joule heating due to the bias should be dissipated by the

TABLE 3-II  
THERMISTOR BOLOMETER CHARACTERISTICS\*

Serial No.	Area mm x mm	Window Material	Time Constant Milli- Second	Responsivity** Volt Watt <sup>-1</sup>	Bias at 25°C Volt	Resistance at 25°C Megohm	Noise N <sub>bias</sub> /N <sub>O</sub> ***	Remarks
BE-2861	0.1x0.1	Ge Lens	5.0	12,500	+ 45	2.39	1.17	Immersed detector Ge lens, 10μ anti-reflection coating.
						2.45	1.17	Compensation thermistor
BE-2536	0.1x0.1	Ge	6.2	13,300	+ 40	2.42	1.15	Ge, window 10μ anti- reflection coating 2 surfaces.
						2.43	1.15	Compensation thermistor

\* Data supplied by Barnes Engineering Co., Stamford, Connecticut.

\*\* Single thermistor flake volts rms per watt average for a 15 Hz square wave incident on bolometer window. Bolometer bridge output is 1/2 this value. Blackbody source temperature +197°C (470°K).

\*\*\* Voltage ratio.

heat sink; the following relationship should be satisfied:

$$\frac{V_p^2}{R_p} = \kappa (T_p - T_o) = \kappa \Delta T \quad (3-6)$$

or solving for  $V_p$

$$V_p = \sqrt{\kappa R_p \Delta T} \quad (3-7)$$

where:

$V_p$  = peak voltage per flake

$R_p$  = thermistor resistance (ohms) at peak voltage

$\kappa$  = thermal conductivity (watts  $^{\circ}\text{K}^{-1}$ ) between  
thermistor and heat sink

$T_p$  = thermistor temperature at peak voltage

$T_o$  = ambient temperature

$\Delta T$  = temperature increment above the heat sink of  
the thermistor flake.

The operating voltage of the thermistor is taken equal to  $0.6V_p$  for the maximum temperature.

Taking the characteristics of the thermistor BE-2861 we obtain:

$$V_p = \frac{45 \text{ volts}}{0.6} = 75 \text{ volts} \quad .$$

Further analysis and computation gives

$$\Delta T = 31^{\circ}\text{C}$$

$$T_p = 273 + 25 + 31 = 329^{\circ}\text{K} \quad .$$

Introducing previous values into Eq. (3-5) we obtain  $R_p = 860,000$  ohms

Introducing the above values into Eq. (3-7) and solving the  $\kappa$ , we obtain the value  $\kappa = 2.14 \times 10^4$  watt  $^\circ K^{-1}$ . With this value of  $\kappa$  we can compute the values of  $V_p$  for any ambient temperature; the operating temperature.

To operate the thermistor over the range of  $-15^\circ C$  to  $20^\circ C$  ( $5^\circ F$  to  $68^\circ F$ ) which is expected at the telescope, we use the circuitry given in Figure 3-18. The bias batteries  $V_A$  and  $V_C$  are 90 V each, the resistors  $R_O$  are 2.4 megohm, the value of the thermistor resistance at  $25^\circ C$  ( $77^\circ F$ ) and the capacitor C are  $14\mu f \times 150$  WVDC (tantalum capacitor).

At  $25^\circ C$  ( $77^\circ F$ ) heat sink temperature ( $20^\circ C$  ambient) the bias applied to each thermistor flake will be 45 V, at  $0^\circ C$  ( $32^\circ F$ ) heat sink temperature, 65 V and at  $-10^\circ C$  ( $14^\circ F$ ) heat sink temperature, 74 V. These values compare very well with the design criteria  $0.6V_p$ .

Table 3-II gives the measured irreducible noise of the thermistor bolometers. When the bias is applied there is an increment in noise of 17 percent over the Johnson noise of the thermistor.

To compute the NEP of the detector, we use the following expressions:

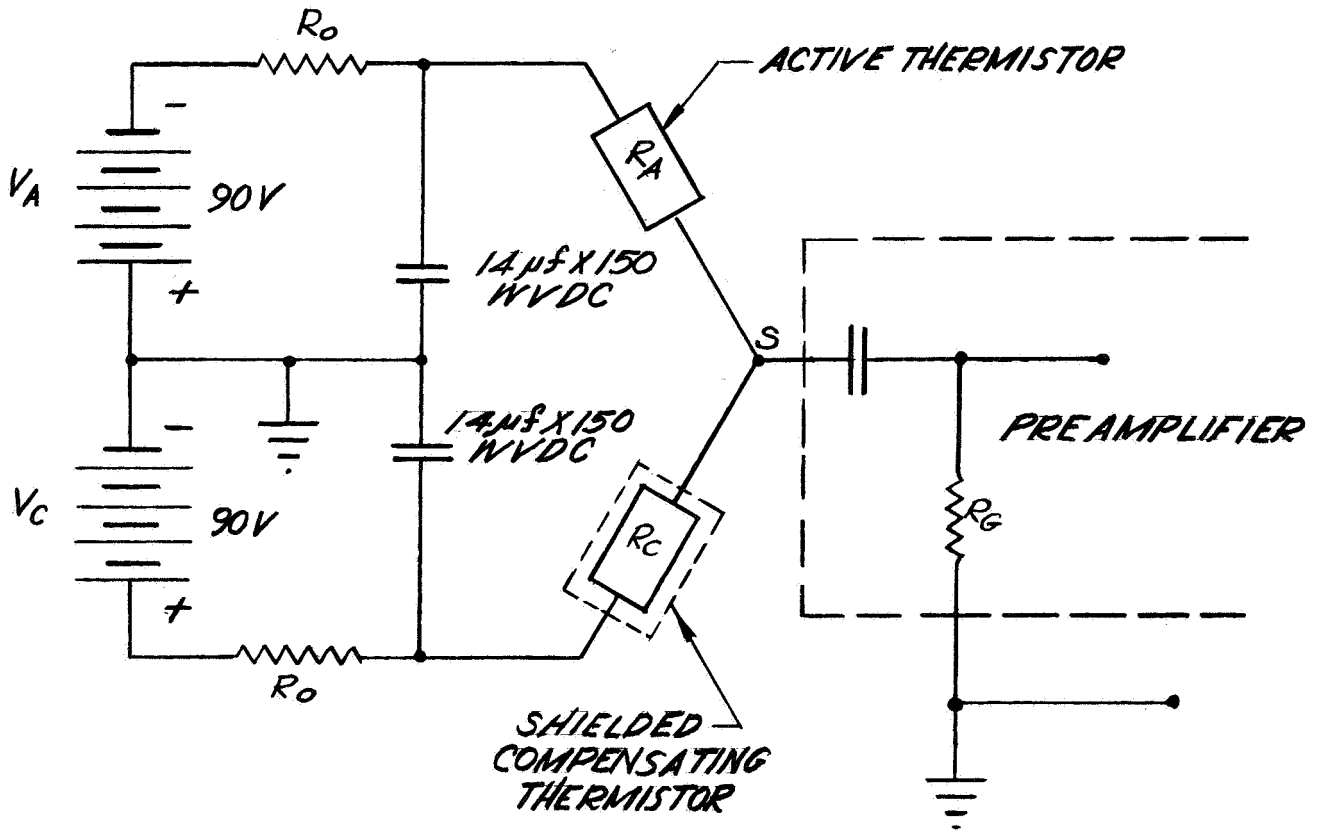
$$NEP = \frac{10^{-10} \sqrt{A}}{\tau} \quad (3-8)$$

for

$$\Delta f = \frac{1}{4\tau} \quad (3-9)$$

where  $A$  = area of the detector in  $cm^2$

$\tau$  = time constant of the detector in seconds.



$$V_A = V_C \quad R_A = R_C \quad R_G \gg R_A \quad R_0 = R_A (25^\circ\text{C}) = R_C (25^\circ\text{C}) = 2.4 \text{ MEG.}$$

FIG. 3-18. Schematic of the circuit used for the thermistor bolometer bridge.

Introducing the proper values from Table 3-II into the above equations and reducing for a bandwidth of 1 Hz, we obtained a NEP of  $2.8 \times 10^{-11}$  watts, equivalent to a voltage noise of  $0.17 \mu\text{V}$  rms. If we compute the Johnson noise of resistors in parallel with a resistance each of  $2.4 \times 10^6$  ohms (resistance of each thermistor) and at  $25^\circ\text{C}$  ( $77^\circ\text{F}$ ), the rms voltage is  $0.14 \mu\text{V}$  for 1 Hz bandpass; if we add the 17 percent increase due to current noise the rms value increased to  $0.17 \mu\text{V}$  which agrees with the values obtained by using Eq. (3-8) and the measurement of the responsivity.

### c.2 Preamplifier

The preamplifier is the Model DP-5A made by Barnes Engineering\*. It has four stages of amplification with substantial feedback to achieve high stability and a reasonable high input impedance.

The circuitry of the preamplifier is given in Figure 3-19. It consists of a p-n-p input stage BE-820, and three stages of amplification using the 2N930 and 2N336 transistors in common-emitter configuration; the last stage uses a 2N3364 transistor in a common-collector configuration.

Standard signal voltages up to 1 V rms injected at the "calibration" terminal will appear as 1 mV signal at the input.

This preamplifier operates between  $-50^\circ\text{C}$  to  $+85^\circ\text{C}$  ( $-58^\circ\text{F}$  to  $185^\circ\text{F}$ ). The power consumption is 2 mA at 24 V dc from a mercury battery power supply.

The  $\pm 1$  db points in the frequency response curve are at 11 and 1,100 Hz. The voltage gain is  $6950 \pm 200$  in the range of  $-40^\circ\text{C}$  to  $+80^\circ\text{C}$  ( $-40^\circ\text{F}$  to  $176^\circ\text{F}$ ), the input impedance 1.5 megohms, the output impedance is less than 500 ohms and the

\* Barnes Engineering Co., "Instrumentation Manual for Transistor Preamplifier, Model DP-5A", December, 1961.



maximum undistorted output is 16 V peak-to-peak.

To determine the source of dominant noise, we recorded the output signal of the pyrometer for three conditions of the input: short-circuited, 1 megohm input resistor (low noise) and the thermistor bolometer connected in the bridge configuration; all records were taken at one second integration time.

### C. Electronic Console

The function of the major panels in the electronic console are described for the purpose of understanding the capabilities and performance of the pyrometer system. In Fig. 3-2 the unit on the right is the electronic console. In this section the panels are listed from the top to the bottom.

#### 1. Voltage Monitor

The voltage monitor panel switch and dc voltmeter allow the operator to measure the operating battery voltages of the preamplifier and phase control rectifier. This is a precautionary measure to assure the constancy of the overall gain of the pyrometer.

#### 2. Phase Controlled Rectifier

Figure 3-20 shows the schematic diagram of the phase controlled rectifier unit. The transistors are all of the field effect type. The two C-653 types are switching types and act as controlled resistances with purely ohmic resistances varying from about  $3 \times 10^3$  ohm at "on" operation to  $1 \times 10^8$  ohm at "off". As these are purely ohmic resistances, they include no offset voltages and the input circuits present a very high impedance to the reference signal so as to effectively isolate it from the output.

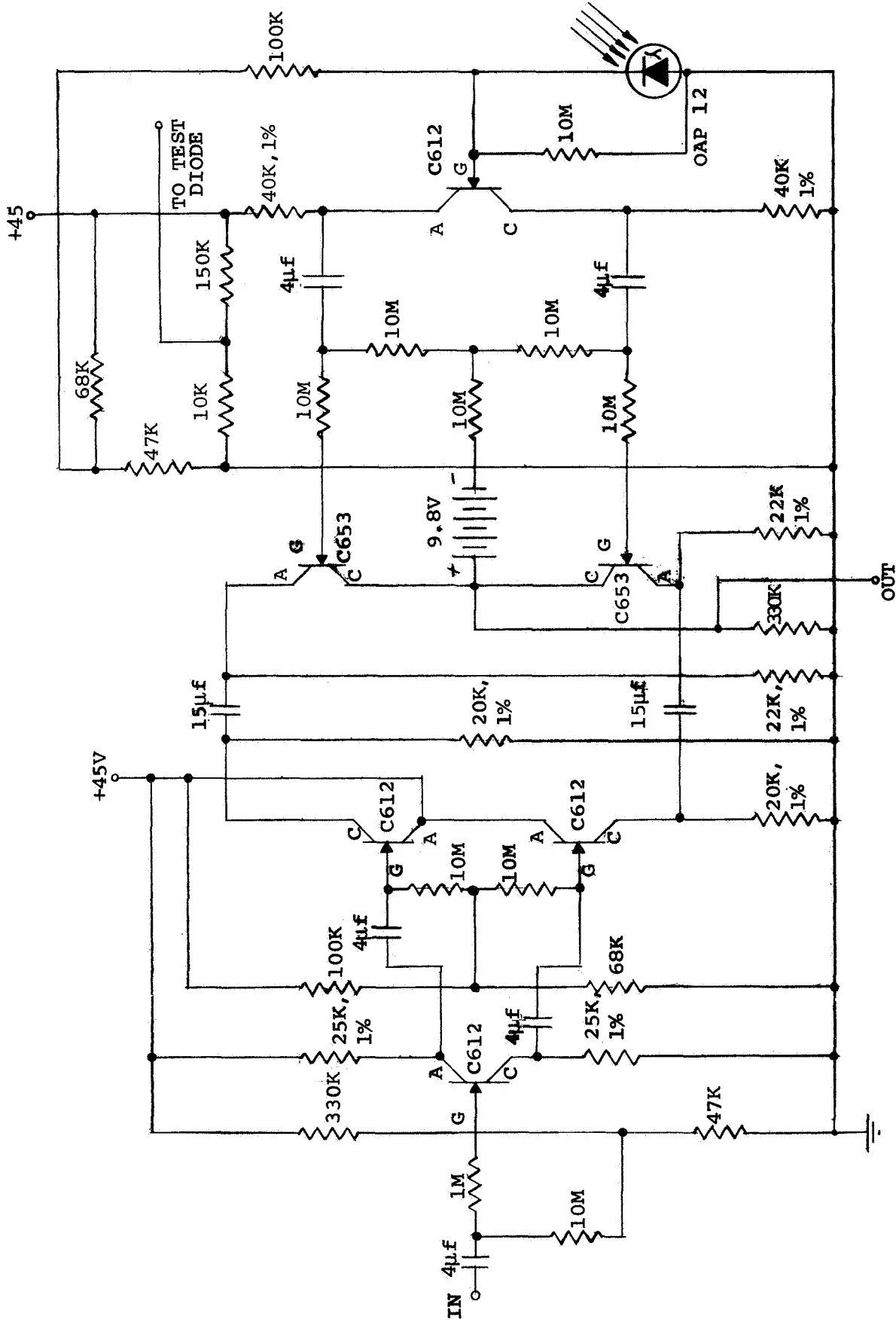


FIG. 3-20. Circuit of the phase controlled rectifier.

Two type C-612 FET's, (whose characteristics resemble those of vacuum tube pentodes), are used as split-load phase inverters, thus permitting single-ended inputs for both the signal and reference inputs. The two remaining C-612's serve as cathode followers to isolate further the signal source and to maintain equal output impedance and preserve symmetry in the output.

The frequency response is limited at the low end of the coupling capacitors, which need not be large because of the high impedance presented by the FET inputs. The high frequency response is limited by the input capacitance of the FET's. Little deterioration of wave-form was observed for square wave inputs from 2.5 to 32 Hz, which is the frequency range of interest.

The high impedance levels maintained throughout permit the elimination of electrolytic capacitors, an important factor affecting reliability. Loading of the source is also kept to a minimum, which simplifies preamplifier design.

The current consumption of the device is about 5 mA from each of the two 45 V batteries. However, examination of the circuit diagram shows that no attempt has been made to minimize current consumption; for instance, the numerous voltage dividers provided could almost all be eliminated, as could the extra 45 V battery, if weight or power requirements warranted it.

As all units are operated in a highly degenerative mode, changes in transistor characteristics have little effect.

To obtain the performance of the phase controlled rectifier, we used a test unit that generates a "signal", and reference voltage to simulate the actual amplified signal from the

thermistor bolometer and the reference signal from the radiation pyrometer head. The frequencies were set to fixed values by means of a pulley and belt arrangement that drives the mechanical chopper. Two germanium photodiodes Amperex OAP12 and the chopped light sources generate the voltages; the phase angle between these sources may vary from  $0^\circ$  to  $180^\circ$ . A picture of the test unit is shown in Figure 3-21.

The oscillograms in Figure 3-22a,b,c,d shows the performance of the phase control rectifier circuit under various input conditions.

### 3. DC Vacuum Tube Voltmeter, Bucking Signal and Time Constant

To amplify the dc signal from the output of the phase controlled rectifier to a sufficient level to drive the paper chart recorder, a Kay Laboratory vacuum tube voltmeter is used.

The Kay Laboratory Model 202A\* microvoltmeter and amplifier is an extremely sensitive high impedance dc vacuum tube voltmeter. The instrument has 14 ranges from  $300\mu\text{V}$  to 1000 V, full scale.

Input resistances for this instrument range from 10 megohm to 100 megohm, depending on what range is being used. The output voltage is  $\pm 1$  V across 2000 ohms.

The instrument consists basically of a preamplifier, 60 cycle ac chopper amplifier, and a dc amplifier with 110 db of gain, stabilized with 40 db of feedback. Following the dc amplifier is a cathode follower circuit employed in a configuration allowing either positive or negative voltage to be displayed on either side of a zero-center meter, without the necessity of meter-reversing switches.

---

\* Kay Laboratory: "Microvoltmeter and Amplifier Model 202A" Instruction Manual.

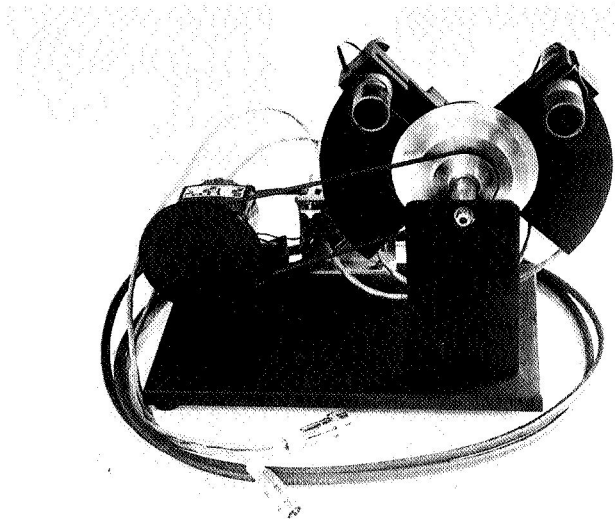


FIG. 3-21. To check the phase controlled rectifier performance, the test unit generates a dummy signal and reference voltages at fixed frequencies and continuous variable phase difference.

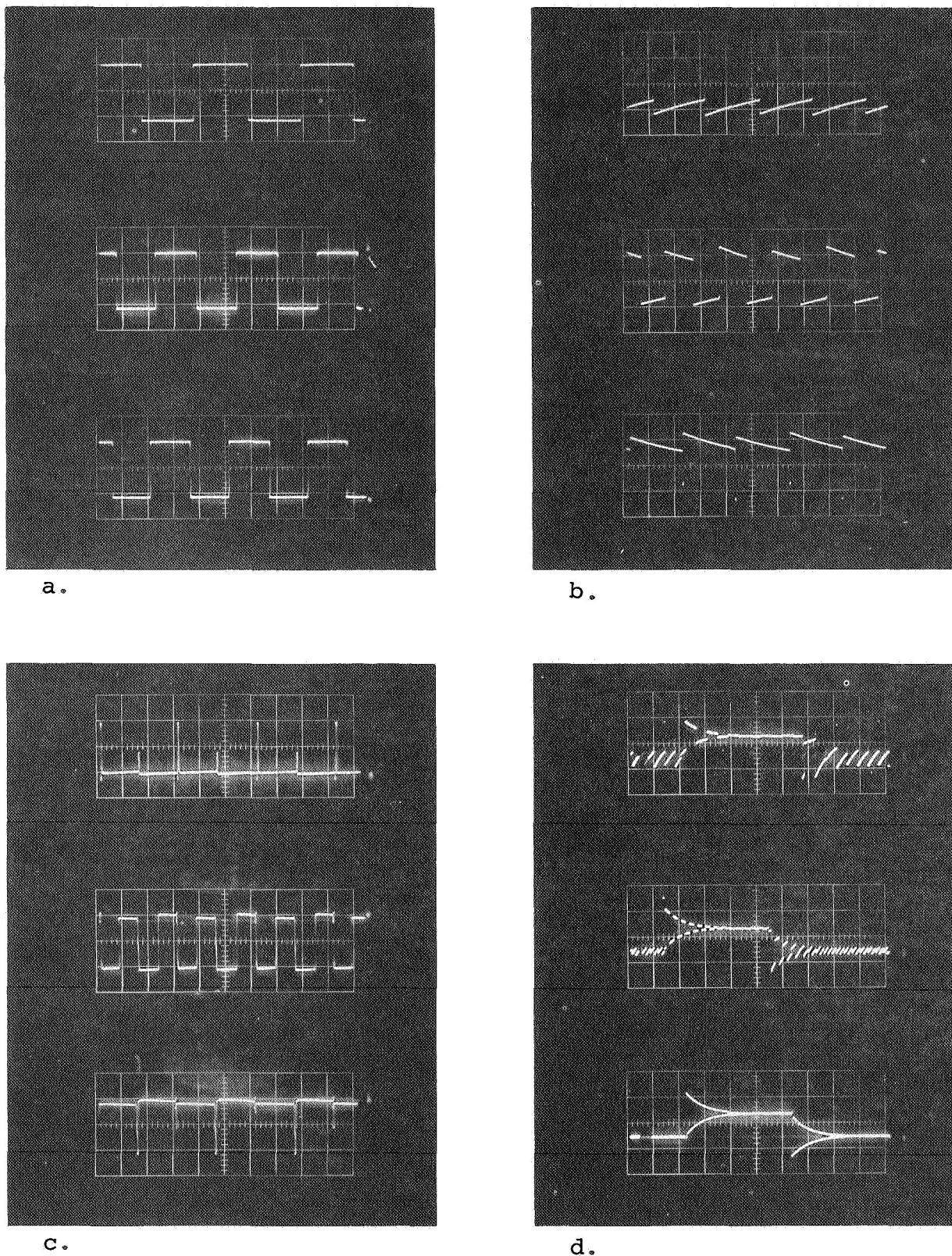


FIG. 3-22. Oscillograms of the input and output signals of the PCR for different conditions of operation: a) input signals from the photodiode at 2.5, 6 and 32 Hz (scale  $1 \text{ V cm}^{-1}$ ); b) output for  $180^\circ$ ,  $270^\circ$  and  $0^\circ$  phase angle difference at 2.5 Hz (scale  $.05 \text{ V cm}^{-1}$ ); c) output for  $80^\circ$ ,  $270^\circ$  and  $0^\circ$  phase angle difference at 32 Hz (scale  $.05 \text{ V cm}^{-1}$ ) and d) response for input step scale  $.05 \text{ V cm}^{-1}$ .

The net overall phase relationship of the instrument amplifier circuitry is that input signal voltage appears as normal when indicated by the output meter.

The inherent circuit noise of this instrument with the input shorted is  $\pm 20\mu\text{V}$ .

The bucking voltage is used to subtract, when needed, the dc level from the pyrometer signal. This allows expansion of the pyrometer scale and recording only the small fluctuations of the infrared signal. Also the bucking voltage allows introduction of known electrical signals into the system and calibration (gain, linearity), at the observing site that can be carried out without the usage of laboratory equipment.

The bucking voltage source is a regulated 5 V power supply Corning Model 8000; the stability is 0.05 percent for a variation in the voltage line of  $\pm 15$  percent. The full range is -2.5 to 0, +2.5 to 0 V and -5.0 to 0, +5 to 0 V; the adjustment is by means of a digital readout potentiometer (999 capacity) giving a resolution of  $\pm 24$  mV per count. The choice of polarity depends upon the temperature of the object being measured; for an object at a temperature lower than the detector a positive bucking signal should be used and vice versa. The equivalent input infrared signal of a bucking signal should be determined for the given operating condition of the pyrometer.

The time constant is set by means of an RC network at the input of the DCVTVM. Non-polarized high-grade capacitors and a fixed value low noise resistor are used in the RC network. The values of the time constant are 0.1, 0.5, 1.0, 2.5 and 5.0 seconds.

#### 4. Paper Chart Amplifier-Recorder

The paper chart amplifier-recorder is a Sanborn single channel Model No. 7701A.

The electronics of the amplifier are fully transistorized.

Inkless recordings are made by a hot-wire writing arm on special heat-sensitive paper. Six inches of recording paper are visible at all times for viewing the record as it is made.

The recorder has two marker arms: one in the right margin of the chart and the other in the left margin. One marker records second and minute signals from the digital clock for precise identification of recorded data. The second arm records a signal from the photographic camera triggered by the shutter mechanism when actuated. The specifications for the recorder relevant to the data reduction are as follows:

Frequency Response: 0 to 125 Hz within 3 db at 10 mm peak-to-peak.

Edge-to-Edge Deflection Writing Arm: 100 mm.

Linearity: Linearity error does not exceed 0.5%.

Gain Stability: Change in gain is less than 0.5% with ambient temperature from 0 C (32 F) to 40 C (104 F) for line voltage change from 103 V to 127 V.

Noise: 0.1 mm peak-to-peak maximum.

Zero Suppression: Positive and negative suppression voltage driven from mercury cells in series with the output of the range switch, and used for both single-ended and balanced input. This provides up to 250 mm (10 in.) of

writing arm deflection at any range position of five times full-scale at maximum setting. Maximum error  $\pm 2\%$  of indicated suppression.

Recording Speeds: Recording speeds available through push-button control are: 0.5, 2.5, 10 and 50.

### 5. Thermistor Thermometer

The temperature of the calibration and reference black-body should be known within  $\pm 0.05^\circ\text{C}$ . Furthermore, the ranges should be  $0^\circ\text{C}$  to  $40^\circ\text{C}$  ( $32^\circ\text{F}$  to  $104^\circ\text{F}$ ) for the calibration and  $-15^\circ\text{C}$  to  $+25^\circ\text{C}$  ( $5^\circ\text{F}$  to  $77^\circ\text{F}$ ) for the reference.

For our application we decided to use as sensor a bead thermistor connected in a constant sensitivity bridge. This type of bridge has been described by Pitts and Priestly<sup>12</sup>. The basic circuitry is given in Fig. 3-23. This is a Wheatstone bridge where  $R$  is the resistance of the thermistor;  $R_a$  are preset potentiometers;  $R_b$  is a high-stability resistor; and,  $A$  is the resistance of the balancing potentiometer,  $Y$  is the resistance of the potentiometer in the bridge circuit, and  $A-Y$  the resistance of the potentiometer in the external circuit. The advantage of this bridge is that when it is balanced at a given temperature, subsequent small changes are measured by the current flowing through the galvanometer as the bridge departs from balance. The current measured is proportional to a small change in resistance.

To compensate for the rate of change of thermistor resistance with temperature, the voltage applied to the bridge is increased when the temperature increases; this is obtained by means of the potentiometer  $A$ . When the bridge is nearly balanced, the following relationship is satisfied:

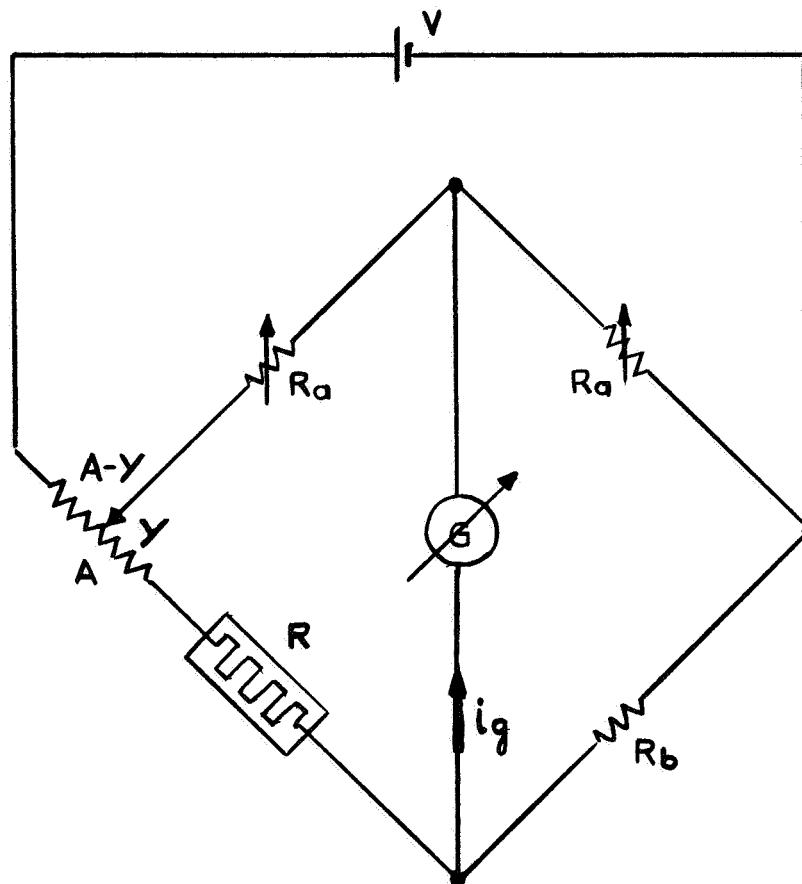


FIG. 3-23. Simplified circuitry of a thermistor constant sensitivity bridge.

$$\frac{di_g}{dT} = \frac{b VR_2}{2R_1 T_2 (2G + R_a + R_1)} \quad (3-10)$$

Where  $R_2$  and  $R_1$  are the resistances of the thermistor at the end of the working range at temperatures  $T_1$  and  $T_2$ , respectively,  $R_a$  is the resistance of the preset potentiometer,  $G$  is the internal resistance of the galvanometer, and  $b$  is the thermistor constant in the following equation:

$$R = a e^{b/T} \quad (3-11)$$

where  $a$  and  $b$  are the constants and  $T$  is the absolute temperature of the thermistor.

Eq. (3-10) is used for the calculations of the sensitivity of the bridge.

The basic bridge shown schematically in Fig. 3-23 is used to measure the temperature of the calibration and reference blackbodies of the radiation pyrometer. In our case, since the range of operating temperatures is rather broad, we have three ranges for the two thermometers. Table 3-III gives the temperature ranges. The interval of the ranges are not equal due to the fact that for the three ranges we use the same balancing potentiometer.

The actual circuit diagram of the thermometers is shown in Fig. 3-24.

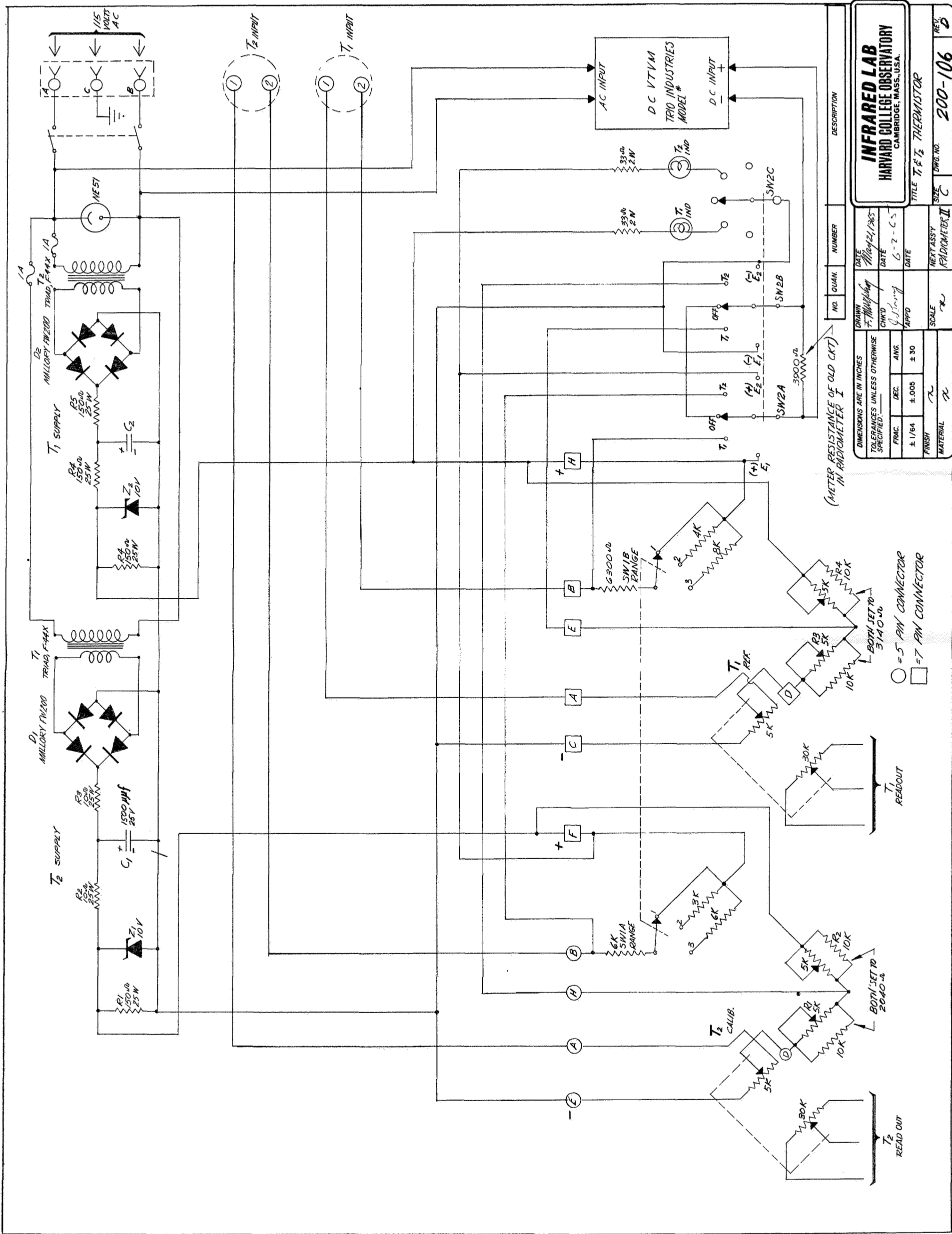


FIG. 3-24. Circuit diagram of the thermistor thermometer to measure the calibration and reference blackbody temperatures.

TABLE 3-III

TEMPERATURE RANGES OF THE CALIBRATION  
AND REFERENCE BLACKBODY THERMOMETERS

Range	Temperature ( $^{\circ}\text{C}$ )			
	Calibration ( $T_2$ )		Reference ( $T_1$ )	
	Max.	Min.	Max.	Min.
I	+42.0	+4.0	+31.5	-4.2
II	+12.5	-1.0	-1.5	-12.0
III	—	—	-12.0	-21.5

Two separate bridge circuits are used for the reference and calibration blackbody thermometers, and both have been calibrated as described in Section IV-C.

To obtain a temperature measurement the bridge is balanced by means of a precision ten-turn potentiometer (balancing potentiometer) coupled to a digital readout counter (999) capacity. The unbalanced voltage of the bridge is measured by a Trio Lab Model 110-1 DC VTVM. This meter has a zero center scale to allow measurement for either  $\pm$  bridge unbalanced voltages.

To read the temperatures, the bridge is balanced by reading zero volts in the three millivolt scale. The minimum unbalanced voltage that could be read is  $\pm 5$  mV. Careful calibration of the thermometer has been carried out from time to time (see Section IV-C). The sensitivity of the thermometers is such that in any scale a change of one digit of the readout counter produces a detectable unbalance of the bridge. For the reference blackbody thermometer one count in the average is equivalent to  $0.035^{\circ}\text{C}$

in scale I,  $0.010^{\circ}\text{C}$  in scale II and  $0.009^{\circ}\text{C}$  in scale III. For the calibration blackbody it will be  $0.038^{\circ}\text{C}$  for scale I and  $0.013^{\circ}\text{C}$  for scale II.

#### 6. Picture Frame Counter and Calibration Blackbody Temperature Adjustment

The 35 mm film used for the photographic channel is 91 m (30 ft.) long; this film does not have the frames numbered. To reduce the photographic data the picture frames have to be identified by sequential numbering; also during operation of the radiometer the operator of the electronics should monitor, indirectly, the film transport of the camera. To achieve both objectives two picture frame counters are used, one in the radiometer head and the other in the electronic console. Both have a capacity of 999 counts. The numbers of the one in the pyrometer head are imaged in one corner of the film using lenses and fiber optics. Both counters are activated by the shutter mechanism every time a picture is secured. At the same time a mark is made on the paper chart recorder to allow later the time identification of the frame (see Fig. 4-2a,b). In the same panel the temperature calibration blackbody adjustment is installed to set the temperature of the body to the appropriate value.

#### 7. Power Distribution

All line voltage controls, fuses and meters have been grouped in this panel. The ac line voltmeter and the elapsed time meter, together with the main power switch are in this section. This section also contains the reticle illumination power supply and brightness control for the pyrometer head, the 12 V dc power supply and meter to drive the photographic camera and frame counter; the switch for the electric motor chopper drive, and the switch to trigger the cameras on the occasion of a special event during observing.

#### D. Monitor Console

The functions of the major panels in the electronic console are described for the purpose of understanding the capabilities and performance of this part of the pyrometer system. In Fig. 3-2 the cabinet on the left is the monitor console. In this section the panels are listed from the top to the bottom.

##### 1. Magnetic Tape Recorder

A Sony TC-600, two-channel magnetic tape recorder with a mixer for each stage is used. This makes it possible to record four channels of information.

These are the verbal report of the observer, the event signal (800 Hz tone), the radio time signals, and the data dictated by the operator of the electronic console during the time that the measurements are carried out.

This recording now serves as a permanent record of all conversations, test conditions and the actual time of each particular observation. The recorded tape is played back in conjunction with the analysis of the data on the paper chart recorder and the projection of the photographic film for a complete data reduction. All frequencies to be recorded fall well within the response of the tape recorder when operating at a recording speed of 3-3/4 ips.

The total recording time at this speed and for a 178 mm (7 in.) reel is approximately two hours. This is accomplished by using magnetic tape "Scotch" type 200-24, and 1/4 inch wide.

##### 2. Digital Clock

In order to reduce the data and to maintain accurate observing time schedules, a digital readout clock has been added to the pyrometer system.

The digital clock, obtained from the Tymeter Clock Company, gives visual readout for hours, minutes, and seconds, for a twenty-four hour period resetting automatically.

The digital clock is provided with switches for closure on second and minute intervals. These switch closures appear as pulses on the paper chart recorder, minutes appearing as four times wider pulses than the seconds and with an amplitude twice as large as the second pulses.

Having both the recorded time pulses and infrared signal on one paper chart simplified data reduction in that the sequence of events can now be easily identified without referring to the time signal recorded on the magnetic tape.

Prior to observing, the digital clock is set to Universal Time with reference to the time signal from radio station WWV by eye and ear.

Periodically during observations, the actual time of each minutes is written on the paper chart as a further aid in data reduction, rather than having to count each individual minute up to the particular point of interest. The start and stop of the recorder is also recorded in the same manner.

### 3. Radio Receiver

A Specific Products Model SR-7 crystal controlled radio receiver is used for reception of time signals from WWV or similar stations.

In the United States the radio receiver is normally used during observations to receive signals from the National Bureau of Standards radio station WWV on either 2.5-25 MHz. When possible, the Dominion Observatory (Canada) Station CHU on

7.3 MHz is used at Agassiz Station (Harvard, Mass.) because of its high signal strength in that area. Other advantages of this station over the WWV type of signal for our application is that every minute is identified by voice.

The time signals are used to set the digital clock from which second and minute signals are recorded on one channel of the paper chart recorder.

Moreover, the time signals from the receiver are recorded on one channel of the magnetic tape recorder.

#### 4. Intercommunications System

Verbal communication between the observer and operator of the electronic equipment is restricted because of reverberations caused by the building. Therefore, two intercommunication systems were installed. The two systems were required to avoid difficulties in operating switches for talk-listen operation required by one system.

The microphones used have sufficient directivity so that feedback between the two intercom systems is minimal. The cabling between the pyrometer head and the rest of the electronics is approximately 27 m (90 ft.). Also, the intercommunication amplifier can be used in connection with the magnetic tape recorder for playback.

#### 5. Event Signal

To indicate the occurrence of an event on the magnetic tape or on the paper chart we used an 800 Hz oscillator. At the pyrometer head and electronic console there are available push-button switches to turn on this event signal by either the observer or the operator. A verbal description after the signal determines the nature of the event.

#### IV. TEST AND CALIBRATION

##### A. Noise Level, Linearity and Drift of the Pyrometer

The noise level, linearity and drift of the radiation pyrometer was measured in our Infrared Laboratory. The pyrometer head was mounted on the infrared bench; the electronic racks were installed also in the same laboratory.

The infrared bench consists of a Barnes Engineering Reference Blackbody model RS-1A, a variable speed chopper, a water tank as a thermal baffle, a series of calibrated stops, a shutter and a recording thermistor thermometer.

The temperature of the reference blackbody cavity was set at 70°C (158°F), the temperature of the room was 22.3°C (72.1°F) and the chopping frequency of the radiation set at 12 Hz. For these measurements which lasted three hours, the laboratory was closed. One person was allowed to enter the laboratory for only a few minutes to read the instruments. This precautionary measure was taken after we observed on previous occasions that the heat generated by one person in the laboratory was enough to increase the temperature of the chopper blades and produced at maximum sensitivity of the pyrometer a detectable drift. We used one second post detection integration time. For the conditions indicated above and using the plug-in unit with the immersed detector BE-2861 and the DP-5A preamplifier, we obtained a peak-to-peak noise level of less than  $6 \times 10^{-11}$  watts. At these power levels we could not detect any drift during a one hour period. Figure 4-1 shows a record of the noise level of the pyrometer. The signal on the detector was  $8.5 \times 10^{-10}$  watts, the post integration time one second and the speed of the paper chart was  $1 \text{ mm sec}^{-1}$ ; the power scale on the paper chart is  $6 \times 10^{-11} \text{ watt mm}^{-1}$ . The record shows that at 5:20 pm the infrared signal was turned to zero and at 5:45 pm the recorder was switched for a few

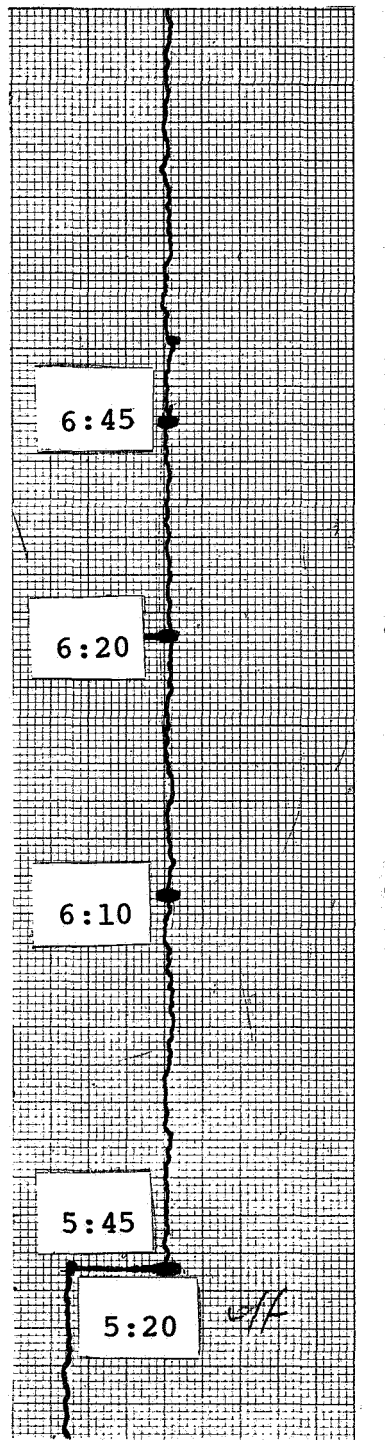


FIG. 4-1. Noise level and drift measurement of the radiation pyrometer.

seconds and stopped; at 6:10 pm it started again. The same sequence of events took place at 6:20 pm and 6:45 pm. The record shows that the peak-to-peak noise level is  $1.3 \times 10^{-10}$  watts, if we reduce this value to 1 Hz bandpass.

#### B. Test of the Pyrometer-Telescope System

The pyrometer, as well as the components and subassemblies, was subjected to thorough tests in the laboratory including environmental tests as a system. We cannot say that the pyrometer was tested on the telescope since it performed the way it did in the laboratory from the time that it was first attached to the telescope.

The scan shown in Figure 4-2a.-b. was obtained at the Newtonian focus of the 155 cm (61 in.) telescope at Agassiz Station during the lunar eclipse, December 18-19, 1964. The telescope was stopped down to f/5.58 by an entrance stop in the pyrometer to ensure that the detector did not "see" anything but the mirror objective. The amount of precipitable water, measured from sounding balloons, was 1.4 mm for one air mass, an exceptionally low value for this observing site.

The post-detection time constant of the pyrometer was 0.2 seconds, and the size of the resolution element was 9" x 9" between half-power points. As the scan shows, the temperature anomalies in Copernicus, Milichius, Galilaei, and an unnamed crater, first become evident as a plus  $\Delta T$ . The incremental temperatures  $\Delta T$  shown in the scan are not corrected for the instrumental profile of the pyrometer. This correction will be important for Milichius, the unnamed crater and Galilaei. The power calibration ( $1.2 \times 10^{-8}$  watts) of the record was obtained with a blackbody calibration.

Figure 4-3 shows a scan from Mare Crisium through Manilius, which was obtained a few hours before the lunar

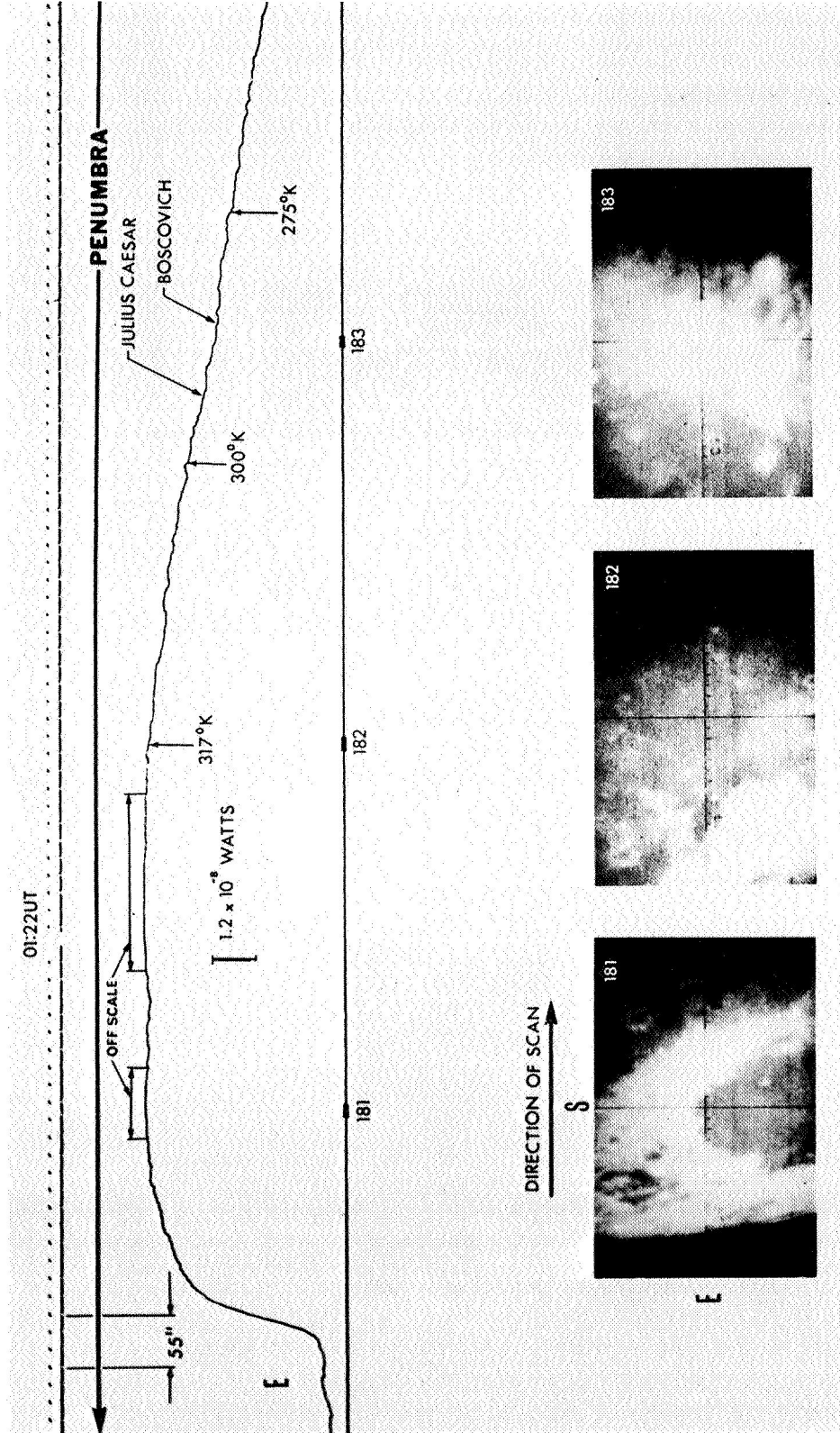


FIG. 4-2a. First part of a complete lunar scan, time identifying pictures, signal marks, and marks indicating when a picture has been secured. Data obtained during the Lunar Eclipse, December 18-19, 1964, with the 155 cm (61 in.) telescope at Agassiz Station. The total amount of precipitable water in the Earth's atmosphere was 1.4 mm. This part of the scan went through an area in penumbra.

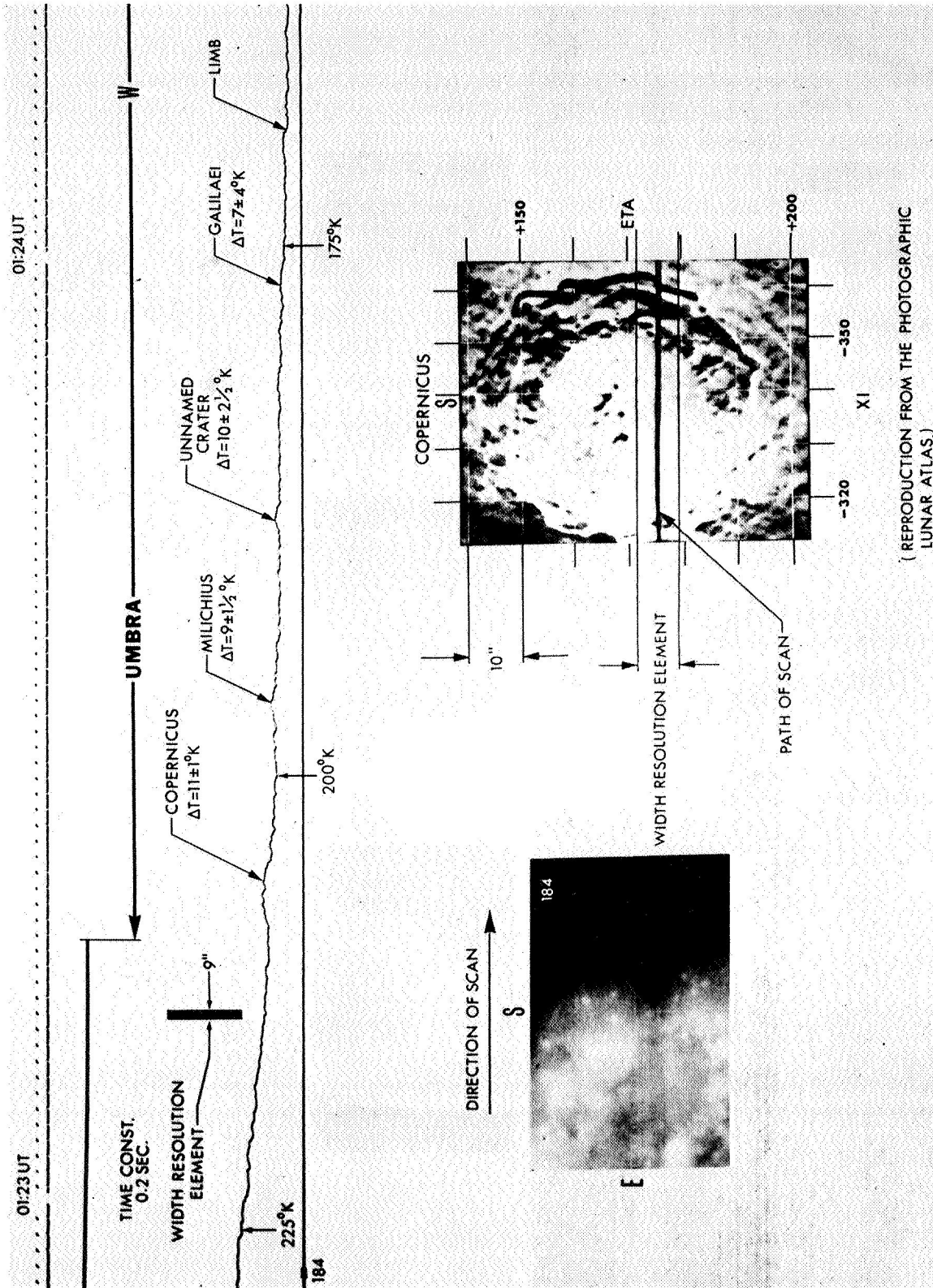


FIG. 4-2b. Continuation of data and scan shown in Fig. 4-2a. This part of the scan passed almost through the Center of Copernicus during the umbral phase. The  $\Delta T$ 's are not corrected by instrumental profile.

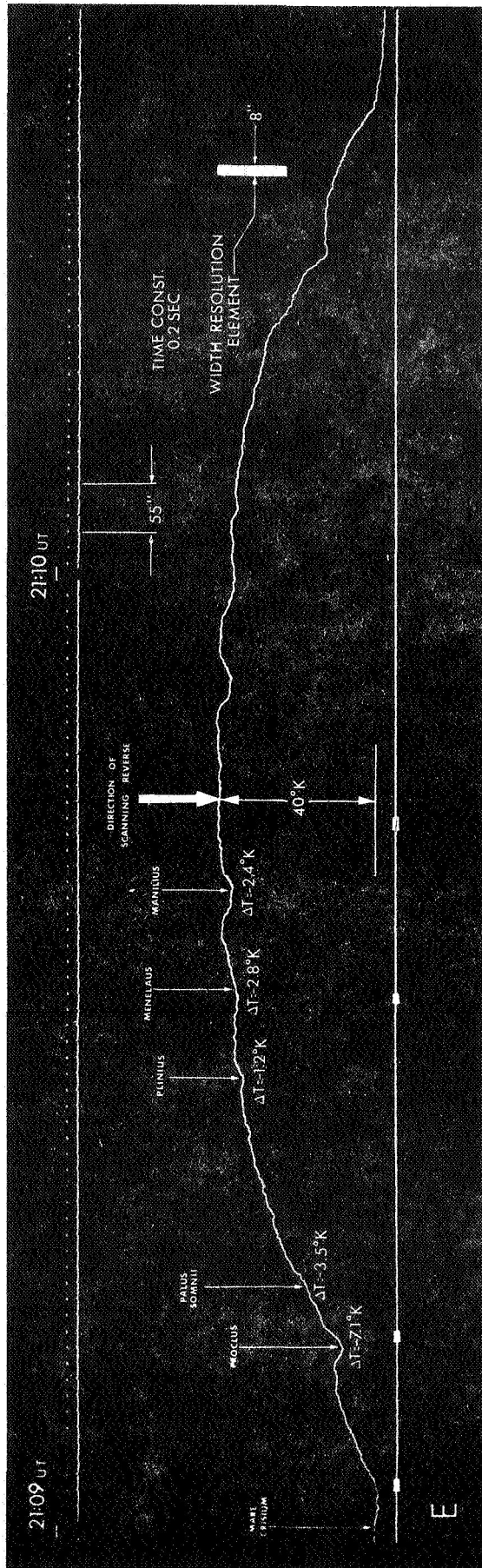


FIG. 4-3. Scan and time marks a few hours before the Lunar Eclipse of June 24-25, 1964, observed from Pretoria (Rep. of South Africa) with the 188 cm (74 in.) telescope. The scan shows several temperature anomalies. To show the validity of the measurements, the direction of scanning was reversed. The second scan shows an almost perfect mirror image of the first scan. The  $\Delta T$ 's are not corrected by instrumental profile.

eclipse of June 24-25, 1964, at the Newtonian focus of the 188 cm (74 in.) telescope at the Radcliffe Observatory (Pretoria, Rep. of South Africa). The amount of precipitable water for one air mass, measured from sounding balloons, was 2.5 millimeters.

The post-detection time constant of the pyrometer was 0.2 seconds and the size of the resolution element was 8" x 8" between half-power points.

To verify that the structure of the scan shown in Figure 4-3 has astrophysical meaning, we reverse the sense of scanning at the point indicated by the arrow. The second part of the scan is almost a perfect mirror image of the first part; the small differences are due to the change in declination of the moon ( $0''.114$  per second of time), which over a minute of time amounts to almost 80 percent of the size of the resolution element. The record shows very clearly the negative increment  $\Delta T$  for the temperature anomalies in Proclus, Plinius and Manilius.

Each one of the event marks indicated at the bottom of the scan shown in Figure 4-3 gives the time at which a picture was secured. The first mark from the left gives the values  $\xi = +0.879$  and  $\eta = +0.276$  as the orthographic coordinates of the center of the resolution element on the moon; at the second mark,  $\xi = +0.700$ ,  $\eta = +0.270$ ; at the third mark,  $\xi = +0.285$ ,  $\eta = +0.253$ ; at the fourth mark  $\xi = +0.065$ ,  $\eta = +0.251$ .

The root-mean square residual in position for this particular scan is  $3''.68$ .

#### C. Blackbody Thermistor Thermometers Calibration

Since our data reduction depends on the calibration of the thermistor thermometers, (reference and calibration

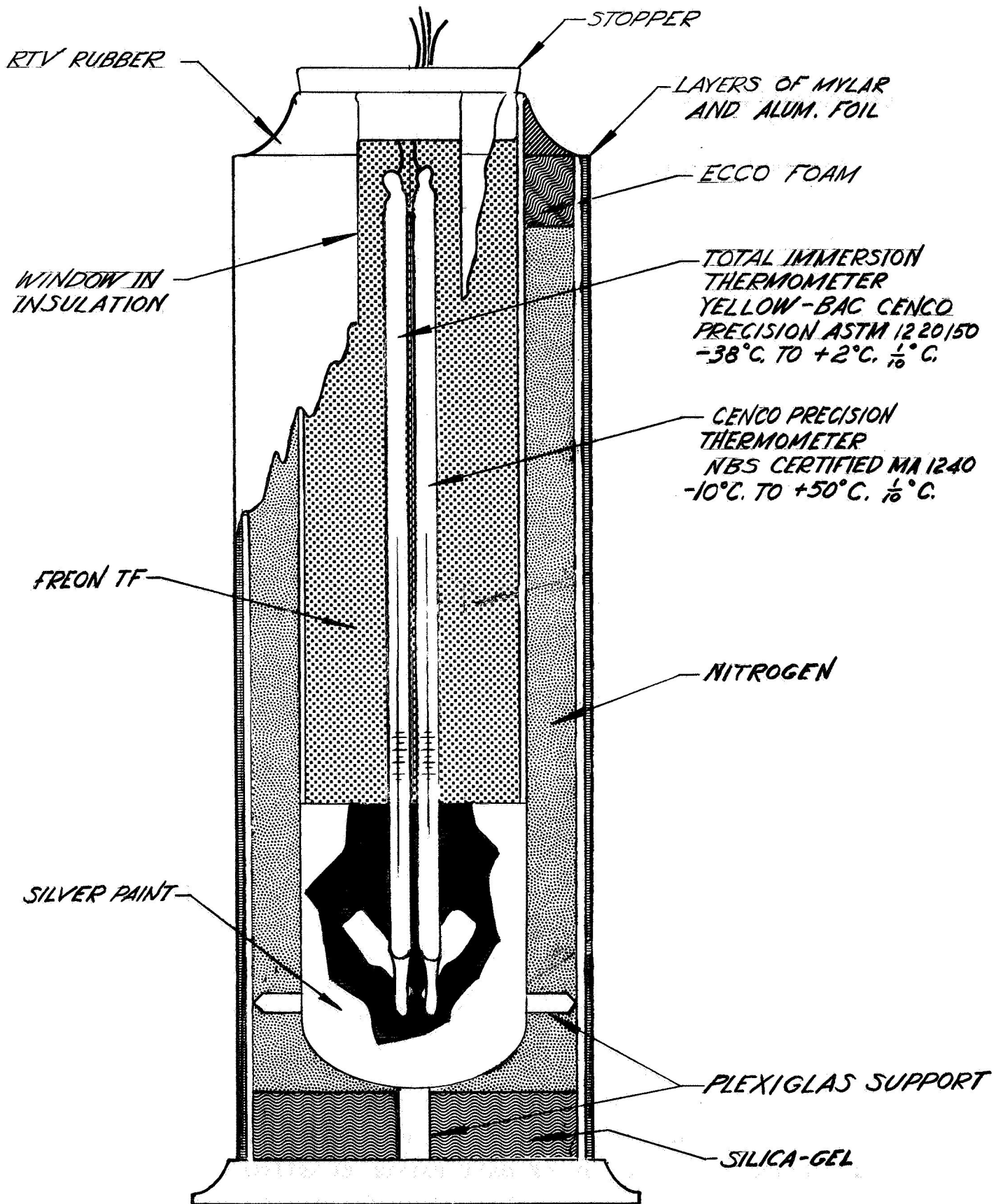


FIG. 4-4. Calibration setup for the thermistor thermometers.

temperatures), we gave the calibration careful attention.

For the calibration, we used two total immersion precision thermometers. One was a Cenco precision thermometer NBS certified (Ma-1240), with  $-10^{\circ}\text{C}$  to  $+50^{\circ}\text{C}$  ( $+14^{\circ}\text{F}$  to  $+122^{\circ}\text{F}$ ) range and  $0.1^{\circ}\text{C}$  divisions. The other was a Cenco precision thermometer ASTM 1220150, with  $-38^{\circ}\text{C}$  to  $+2^{\circ}\text{C}$  ( $-36.4^{\circ}\text{F}$  to  $+35.6^{\circ}\text{F}$ ) range, and  $0.1^{\circ}\text{C}$  divisions.

The two thermistor units under calibration were attached to the tip of the thermometers and fully immersed in liquid Freon-TF as indicated in Figure 4-4. The inner tube was mounted inside another glass tube. The separation between the tubes was achieved by a vertical supporting rod at the bottom and three rods equally spaced around the sides near the base; all were made of Plexiglas.

The spacer at the upper part of the tube was made of Eccofoam and sealed with Silicone rubber. To avoid condensation of moisture at low temperatures, the space between the two glass tubes was filled with nitrogen and at the bottom silica gel was added. To minimize coupling by radiation between the inside of the inner tube and the surroundings of the outside tube, the lower part of the inner tube was wrapped with a sheet of Mylar, a layer of aluminum foil, and another sheet of Mylar, a layer of aluminum foil, and another sheet of Mylar. There is a small window in the wrappings to allow for the reading of the thermometers.

Before the thermistor thermometers were calibrated, the thermistor was subjected to several temperature cycles. This was at extreme temperatures of calibration to allow for any aging effect; however, we are planning a systematic check of the calibration of the thermistors.

The calibration procedure was as follows:

1. The Freon was cooled down to  $-39^{\circ}\text{C}$  ( $-38^{\circ}\text{F}$ ) then transferred to the calibration container, which is pre-cooled in an environmental chamber.
2. Both thermistor assembly units were attached to the certified thermometers and immersed in the cooled Freon.
3. The Freon was stirred for one minute.
4. After stirring, we waited for approximately twenty minutes to allow for thermal equilibrium between the bath, the thermometers, and the thermistor assemblies.
5. A null of the bridge and the reading of the counter was taken for every  $0.25^{\circ}\text{C}$  ( $0.45^{\circ}\text{F}$ ) intervals. The thermometer was read with the aid of a magnifier.

No stirring or agitation took place during the calibration.

It took 2.5 hours for the temperature of the bath to rise from  $-35^{\circ}\text{C}$  ( $-31^{\circ}\text{F}$ ) to  $0^{\circ}\text{C}$  ( $32^{\circ}\text{F}$ ), and approximately 4 hours for it to rise from  $0^{\circ}\text{C}$  ( $-32^{\circ}\text{F}$ ) to  $23^{\circ}\text{C}$  ( $73^{\circ}\text{F}$ ).

In two calibration runs, in the range of  $-35^{\circ}\text{C}$  ( $-31^{\circ}\text{F}$ ) to  $23^{\circ}\text{C}$  ( $73^{\circ}\text{F}$ ), we achieved a consistency better than  $\pm 1$  division of the counter.

For higher temperature ranges, the bath was heated to  $41^{\circ}\text{C}$  ( $105^{\circ}\text{F}$ ) and readings were secured every ten or fifteen minutes at first and then every 30 to 45 minutes during the cooling to  $23^{\circ}\text{C}$  ( $73^{\circ}\text{F}$ ).

REFERENCES

1. H. C. Ingrao, D. H. Menzel and A. Burke, "Study of Infrared Instrumentation for Thermal Photography of the Moon", Scientific Report No. 1, NASA Grant NSG 64-60, Harvard College Observatory, May 15, 1964.
2. H. C. Ingrao and D. H. Menzel, "Instrumentation for Observations of Planets in the Far Infrared", Mémoires Soc. R. Sc. Liège, cinquième série, Vol. 24, tome VII (1962).
3. H. C. Ingrao, F. J. Kahn and D. H. Menzel, "Ferroelectric Bolometer for Space Research", Proceedings of the 5th International Symposium on Space Technology and Science, Tokyo, Japan, September 1963.
4. H. C. Ingrao, F. J. Kahn and D. H. Menzel, "Ferroelectric Bolometer for Space Research", Scientific Report No. 3, NASA Grant No. NSG 64-60, November 1, 1963, Harvard College Observatory.
5. M. M. Benarie, "Optical Pyrometry Below Red Heat", JOSA, Vol. 47, No. 11, November 1957, pp. 1005-1009.
6. C. E. Mendenhall, "On the Emissive Power of Wedge-shaped Cavities and Their Use in Temperature Measurement", Ap. J. Vol. 33, No. 2, March 1911, p. 91.
7. J. F. Grainger and J. Ring, "The Luminescence of the Lunar Surface" Chapter 10, Physics and Astronomy of the Moon, (ed.) Kopal, (Academic Press, New York) (1962).
8. G. V. Coyne, "Comparative Spectrophotometry of Selected Areas on the Lunar Surface", Astron. J., Vol. 68 (1963). p. 49.
9. W. H. Brattain and J. A. Becker, "Thermistor Bolometers", JOSA, Vol. 36, (1946) p. 354.
10. E. W. Wormser, "Properties of Thermistor Infrared Detectors", JOSA, Vol. 43 (1953) pp. 15-21.
11. R. DeWaard and E. W. Wormser, "Thermistor Infrared Detectors, Part I, Properties and Developments", USDC, Office of Technical Services NAVORD 5495, 30 April, 1958.
12. E. Pitts and T. Priestley, "Constant Sensitivity Bridge for Thermistor Thermometer", J. Sci. Instr., Vol. 39, (1962) pp. 75-77.

### ACKNOWLEDGMENTS

This work was sponsored by the National Aeronautics and Space Administration under Grant No. NsG 64-60.

We wish to thank Mr. N. W. Cunningham, former Acting Head, Lunar Sciences, NASA, and Mr. Roger Moore, former Head of Planetary Sciences, NASA, for their continued encouragement throughout this program.

Acknowledgment is also due to Mr. Anthony Burke, graduate student and Mr. Daniel Malaise, NASA International Fellowship (Astrophysical Institute, Liege, Belgium).